ORIGINAL PAPER - PRODUCTION ENGINEERING

CrossMark

A numerical modelling and simulation of core-scale sandstone acidizing process: a study on the effect of temperature

Van Hong Leong[1] · Hisham Ben Mahmud[1] · Ming Chiat Law[2] · Chee Yew Henry Foo[1] · Inn Shi Tan[1]

Abstract

A wide and comprehensive understanding of the chemical reactions and mechanisms of HBF_4 is crucial as it significantly influences its performance in stimulating a sandstone formation. In general, it is well-known that HBF_4 is able to provide a deeper penetration into the sandstone matrix before being spent due to its uniquely slow hydrolysis ability to produce HF. In the present study, a 3D numerical modelling and simulation were conducted to examine the capability of HBF_4 in enhancing the porosity and permeability of the sandstone matrix. The model is built in COMSOL® Multiphysics commercial software of computational fluid dynamics (CFD) to simulate the acid core flooding process on sandstone core. The model had been validated against the experimental data in the literature. The results matched with the measured plot data very well. The effect of temperature on the performance HBF_4 sandstone acidizing is evaluated in this study. The simulation results indicated that at low temperature of 25 °C, HBF_4 is not very effective, as justified in its poor porosity and permeability increments of only 1.07 and 1.23, respectively. However, at elevated temperatures, the porosity and permeability enhancement also become increasingly more significant, which showed 1.26 and 2.06, respectively, at 65 °C; and 1.67 and 7.06, respectively, at 105 °C. Therefore, one can conclude that HBF_4 acid treatment performed better at elevated temperatures due to increased hydrolysis rate, which is a governing function in HBF_4 sandstone acidizing. Overall, this model had provided a reliable alternative to optimize various other parameters of HBF_4 acid treatment.

Keywords Well stimulation · Sandstone matrix acidizing · Fluoroboric acid · Computational fluid dynamics (CFD) · Finite element analysis (FEM)

Abbreviations

3D	Three-dimensional
CFD	Computational fluid dynamics
FEM	Finite element method
HBF_4	Fluoroboric acid
HBF_3OH	Borofluoric acid
$HBF_2(OH)_2$	Dihydroxyfluoroboric acid
$HBF(OH)_3$	Trihydroxyfluoroboric acid
H_3BO_3	Boric acid
HF	Hydrofluoric acid
HCl	Hydrochloric acid
H_2SiF_6	Fluorosilicic acid
$Si(OH)_4$	Silica gel
AlF_3	Aluminum fluoride
H_2O	Water
H^+	Hydrogen ion
BF_4^-	Fluoroborate ion
vol	Volume
MOHE	Ministry of higher education
FRGS	Fundamental research grant scheme
FOES	Faculty of engineering and science

Units

1	Dimensionless
%	Percentage
°C	Degree celsius
°K	Degree kelvin
psi	Pounds per square inch
Pa	Pascal
Pa s	Pascal second
s	Second
min	Minute
in	Inch
m^2	Meter square

✉ Hisham Ben Mahmud
  leongvanhong@postgrad.curtin.edu.my

[1] Petroleum Engineering Department, Curtin University, CDT 250, 98009 Miri, Sarawak, Malaysia

[2] Mechanical Engineering Department, Curtin University, CDT 250, 98009 Miri, Sarawak, Malaysia

مدينة الملك عبدالعزيز
KACST للعلوم والتقنية

۩ Springer

m/s	Meter per second	ϕ_1	Porosity at time step 1 [1]
m^2/s	Meter square per second	ϕ_2	Porosity at time step 2 [1]
g	Gram	ϕ^0	Initial porosity [1]
1/m or m^{-1}	Per meter	ϕ_f	Final porosity [1]
g/m^3	Gram per meter cube	k	Permeability [m^2]
kg/m^3	Kilogram per meter cube	k_1	Permeability at time step 1 [m^2]
g/m^{3}s	Gram per meter cube second	k_2	Permeability at time step 2 [m^2]
g/mol	Gram per mol	k_0	Initial permeability [m^2]
mol/m^3	Mol per meter cube	k_f	Final permeability [m^2]
mol/m^{2}s	Mol per meter square second	r_h	Hydrolysis rate of HBF$_4$ [mol/m^{3}s]
mol/m^{3}s	Mol per meter cube second	k_h	Equilibrium rate constant [1/s]
mD	Milli Darcy	M_1	Lumped group of fast-reacting minerals [1]
cal/mol.°K	Calories per mol degree kelvin	M_2	Lumped group of slow-reacting minerals [1]

Subscripts

x	x-direction/x-axis
y	y-direction/y-axis
z	z-direction/z-axis
i	Type of acids (1 = HF, 2 = H$_2$SiF$_6$)
j	Type of minerals (1 = fast-reacting mineral, 2 = slow-reacting mineral, 3 = silica gel)

List of symbols

e	Exponential function [–]
∂	Partial differential function [–]
$\overline{\nabla}$	Divergence function [–]
$\sum$	Summation function [–]
R	Universal gas constant [cal/mol °K]
γ	Ratio of gravity [1]
t	Time [s or min]
T	Temperature [°C or °K]
P	Pressure [Pa]
P_0	Initial pressure [Pa]
P_f	Final pressure [Pa]
P_{out}	Back pressure at the outlet of the core [Pa]
P_{ref}	Reference pressure level [Pa]
ΔP	Pressure drop [Pa]
Δx	x distance of control volume [m]
Δy	y distance of control volume [m]
Δz	z distance of control volume [m]
Δt	Change in time [s or min]
μ	Viscosity of acid [Pa s]
$\propto$	Viscosity of acid [Pa s]
D_c	Diffusion coefficient of acid [m^2/s]
v_i	Stoichiometry coefficient of reactions [1]
$v_1 - v_8$	Stoichiometry coefficient of reactions [1]
u	Velocity of injected acid [m/s]
$\bar{u}$	Vector velocity [m/s]
u_x	Average Darcy velocity in y–z plane [m/s]
u_y	Average Darcy velocity in x–z plane [m/s]
u_z	Average Darcy velocity in x–y plane [m/s]
v	Injection rate of acid [m/s]
Q	Injection rate of acid [m/s]
ϕ	Porosity [1]

M_3	Silica gel [1]
$K_{Si(OH)_4}^{SP}$	Solubility product of silica gel [1]
C_i	Concentration of acid [mol/m^3]
C_i^0	Initial concentration of acid [mol/m^3]
C_{acid}	Concentration of acid [mol/m^3]
C_3	Concentration of HBF$_4$ [mol/m^3]
C_{HBF_4}	Concentration of HBF$_4$ [mol/m^3]
C_{HF}	Concentration of HF [mol/m^3]
$C_{H_2SiF_6}$	Concentration of H$_2$SiF$_6$ [mol/m^3]
C_{H^+}	Concentration of hydrogen ion [mol/m^3]
$C_{BF_4^-}$	Concentration of fluoroborate ion [mol/m^3]
v_{acid}	Volume of acid [m^3]
$v_{mineral}$	Volume of mineral [m^3]
V_j	Volume fraction of mineral [1]
V_1	Volume fraction of fast-reacting mineral [1]
V_2	Volume fraction of slow-reacting mineral [1]
V_3	Volume fraction of silica gel [1]
V_1^0	Original volume fraction of fast-reacting mineral [1]
V_2^0	Original volume fraction of slow-reacting mineral [1]
V_3^0	Original volume fraction of silica gel [1]
$N_{a,j}$	Number of acids reacting with minerals $j=2$ [1]
N_m	Total number of minerals reacting with acids $i=3$ [1]
$E_{f,i,j}$	Reaction rate between the acid and mineral [m/s]
S_j^*	Reaction surface of mineral [1/m]
MW_i	Molecular weight of acid i [g/mol]
MW_{acid}	Molecular weight of acid [g/mol]
$MW_{mineral}$	Molecular weight of mineral [g/mol]
ρ	Density of acid [kg/m^3]
ρ_{acid}	Density of acid [kg/m^3]
ρ_j	Density of mineral j [kg/m^3]
ρ_s	Density of solid [kg/m^3]
$\beta_{i,j}$	Dissolving power of mineral j by acid i [1]
n	Coefficient of sandstone condition = 3 [1]

l or L	Length of core sample [in]
r	Radius [in]
r_c	Radius of core sample [in]
D	Diameter of core sample [in]
W_i	Overall mass of component i in the control volume [g/m^3]
$\omega_{i,j}$	Mass fraction of component i in phase j [1]
$\omega_{i,s}$	Mass fraction of component i in solid phase [1]
g_i	Mass of component i [g]
$g_{\text{phase } j}$	Mass phase j [g]
g_{solid}	Mass solid phase [g]
St_j	Saturation of phase j [1]
N_i	Flux of component j [m/s]
u_j	Darcy velocity of phase j [m/s]
$K_{i,j}$	Dispersion coefficient of component i in phase j [1]
R_i	Source of component i [g/m^{3}s]
r_i	Surface area—specific reaction rate of i [mol/m^{2}s]
S_j	Surface area of mineral j in a unit of bulk volume [1/m]
N_{Da}	Damkohler number [1]
Λ	Dimensionless composition of mineral [1]
N_{Ac}	Dimensionless acid capacity number [1]

Introduction

Sandstone acidizing treatment fluids

In the context of petroleum exploration, the maturity and diagenesis process of a sandstone reservoir will significantly affect and determine its initial porosity, hence characterizing the initial quality of the reservoir. This is more related and attributed to the geological process. Therefore, a full understanding of the geological history and diagenetic processes of a sandstone reservoir is of paramount importance, especially for tight sandstone reservoir (Lin et al. 2017). However, entering the later stage of petroleum production, enhanced oil recovery technique such as sandstone acidizing played a major role in well stimulation (Leong and Ben Mahmud 2017).

Formation damage is one of the major problems in sandstone reservoirs. It would normally cause rapid declination in well production. It is caused by various reservoir operations such as drilling, completion and production (McLeod 1984). Sandstone acidizing is one of the most effective method to enhance the recovery of a damaged well by increasing the permeability of the formation (Leong and Ben Mahmud 2018). Mud acid is a combination of hydrofluoric acid (HF) and hydrochloric acid (HCl). It had been used to stimulate sandstone reservoir commonly due to its high reactivity with various sandstone minerals such as quartz, feldspar and clays (Smith and Hendrickson 1965).

However, mud acid also caused some negativity to the wells such as rapid reaction rate with the formation at high temperature condition. This had resulted in shallow penetration distance and corrosion. In worst case scenario, this also contributed to production loss (Leong and Ben Mahmud 2018). Therefore, many other chelating agents and alternative acids had been developed such as the fluoroboric acid and organic acid (Shafiq and Ben Mahmud 2017). In this study, the technical performance of HBF$_4$ had been studied intensively.

Fluoroboric acid (HBF$_4$) has a unique slow hydrolysis reaction to produce hydrofluoric acid (HF). Its hydrolysis process is, however, a function of temperature and concentration (Ryss 1956). Wamser (1948, 1951) carried out investigation on the hydrolysis of HBF$_4$ at room temperature condition to produce HF. Based on the result, the equilibrium constant of HBF$_4$ is determined to be 2.3×10^{-3} [1] at room temperature. Thomas and Crowe (1978, 1981) applied HBF$_4$ to stimulate the sandstone reservoirs. HBF$_4$ had demonstrated its efficiency in enhancing the penetration of live acid as well as stabilizing the clays.

Bertaux (1989) tested on the use of 8% HBF$_4$ on sandstone that contained K-feldspar. It was indicated that the precipitate, KBF$_4$ formed did not damage the sandstone. So, HBF$_4$ had demonstrated enhanced sandstone permeability. On the other side, the precipitate, K$_2$SiF$_6$ formed resulted in reduced sandstone permeability significantly.

Moreover, after being treated with HBF$_4$, Paccaloni and Mauro (1993) reported a successful 5 years production of a silt and clay damaged well caused by mud acid previously. Meanwhile, Kume et al. (1999) showed that the adoption of HBF$_4$ in treating the Niger Delta wells caused a mixture of both positive and negative results. Some well's permeability was not only unimproved, but also reported to be reduced. Restrepo et al. (2012) combined the use of HBF$_4$ with the organic acids. Based on the result, a deep live acid penetration is obtained while minimizing the secondary and tertiary precipitation reaction.

Modelling technique of sandstone acidizing process

According to the review of literature data, vast amount of experiments had been conducted on the performance of HF and HBF$_4$. However, it is obviously seen that less effort had been made in the development of model for HBF$_4$ acidizing (Leong et al. 2018). To discover appropriate modelling strategy for HBF$_4$ acidizing, there are a number of HF acidizing models which could be referred as a modelling technique. Overall, there are four type of model that had been developed in the past by researchers on HF acidizing, namely, the lumped-parameter model, two-parameter model,

four-parameter model and detailed-chemistry model (Al-Shaalan and Nasr-El-Din 2000).

Schechter and Gidley (1969) developed a lumped-parameter model to study the influence of surface reactions of a porous sandstone. Basically, this is the simplest model developed in the past as the model simplified all the acid–mineral chemical reactions into one generalized equation: HF + Minerals → Products. The model included the distribution of pore space in the sandstone matrix and the surface reactions. This model has low accuracy in predicting the movement of acid front since the experimental results were two to three times higher than the modelling results. This is mainly due to the oversimplification of the acid–mineral chemical reaction. Different minerals such as quartz, feldspars and clays have different reactivity and must be considered separately.

Later, Hekim et al. (1982) presented a two-parameter model, which involved different rate of dissolution for different minerals. Two groups of minerals were classified together, being feldspars and clays as the fast-reacting minerals; and quartz being the slow-reacting minerals. This model gained popularity as it can predict the variation in permeability. However, the reactivity of fluorosilicic acid, H_2SiF_6, which is a by-product formed in situ was neglected. The secondary reaction between H_2SiF_6 with the fast-reacting minerals would result in silica gel precipitation had been overlooked in the two-parameter model.

Hereafter, the development of a four-parameter model was made by Bryant (1993), which had taken the precipitation of silica gel into consideration. The secondary reaction had been considered in the model as well. This model had later become a useful basis for many other researchers to predict the HF acid performance in sandstone acidizing over many years. When compared to the previous model, this four-parameter model demonstrated a higher accuracy in predicting the change in porosity and permeability after HF acidizing in sandstone matrix.

Sevougian et al. (1995) made an attempt by developing a detailed-chemistry model. Although this model is also presented based on the reaction kinetics of minerals, it considered different kinds of minerals individually. In this model, a total of 7 elements, 13 minerals and 13 species were included. The modelling results indicated that this model had shown close validation with the experimental data at high rate of acid injection. Nevertheless, this model is far from accurate in predicting acidizing for low rate of acid injection. Overall, this model that treated the chemical reactions in a much complex way failed to bring advancement in the sandstone acidizing prediction. This is mainly due to over complication of the model reactions. Therefore, the four-parameter modelling approach had been adopted in present work for HBF_4 acidizing.

In this study, a 3D core-scale numerical model is developed to simulate the process of HBF_4 core flooding in a sandstone. A number of simulation sets were conducted using the application of COMSOL® Multiphysics commercial software in CFD. The model considered the hydrolysis process of HBF_4, the chemical reactions between acids and minerals; and many other governing equations in it. The pressure based on Darcy equation, material conservation of acids and mineral components, porosity change and permeability change were modelled. Reasonable assumptions were made for model simplification purpose. The important input parameters in describing the sandstone core flooding process were input and set based on the experimental environments so that the model can be validated.

By utilizing this model, the acid transport in porous medium was simulated to investigate the performance of HBF_4 in enhancing the porosity and permeability of a sandstone core. In present work, the effect of temperature on HBF_4 acidizing was determined by conducting the simulation at various temperatures such as 25, 45, 65, 85 and 105 °C. This numerical method allowed a cost and time saving alternative to simulate HBF_4 acidizing process, although different numerical simulations had their own sets of limitation. Furthermore, this method is also very beneficial and useful to perform sandstone design and optimization of various other parameters that would significantly affect the HBF_4 acidizing performance such as the acid injection rate, acid concentration and mineral volume fraction.

Overall, this paper had extended the boundary of sandstone acidizing research area by extensively studying the effect of elevated temperature up to 105 °C to increase the porosity and permeability of a sandstone formation, which had been lacking in the literature. Also, this paper presented the integrated modelling and simulation of sandstone acidizing process with the use of COMSOL Multiphysics besides incorporating the model of HBF4 with the previous HF model.

HBF_4 numerical model development

Based on the literature review, there had been many applicable models that were developed based on commonly known hydrofluoric, HF acidizing process. However, there is limited focus of numerical studies on fluoroboric, HBF_4 acidizing. Hence, in this research, a general numerical model that is specifically focusing on HBF_4 sandstone acidizing is presented. This model is developed based on the mud acid acidizing modelling approach by Li et al. (2004). The HBF_4 model has been developed based on the Finite Element Method (FEM). One of the key features of FEM is that it is applicable to unstructured mesh. In terms of the geometry used, FEM is also more flexible. The model is developed based on the kinetics and reaction mechanism of the acids and minerals. Empirical correlation had been used

to calculate the equilibrium between the different aqueous species. The detail description of the model is discussed in the next sections.

Model description and governing equations

A three-dimensional (3D) model had been developed to simulate the sandstone acid treatment process, also known as the core flooding process. The main physics that had been considered in the model included the Darcy's law, mass conservation or transport of acids and minerals and the overall mass balance equations. There are a number of assumptions that were made to describe the acidizing process in a simplified way. The assumptions that were considered in the model are as follows:

I. Single phase flow
II. Incompressible fluid and rock
III. Only liquid phase (the acid) and solid phase (the mineral) present
IV. No dispersion
V. No sorption on solid phase
VI. No effects of gravity

Chemical reaction model

In fact, the chemical reactions between the acids and minerals are very complex if they were to be considered independently in a model. This is because there is a large number of mineral components present in a sandstone matrix. Therefore, it is rare to represent these entire chemical reactions separately. Commonly, the reacting minerals in the sandstone were being classified and lumped into several groups according to their reactivity with the acids. In other words, minerals having the similar reaction rate while reacting with the acids would be lumped together.

In the formerly developed two-parameter model, the minerals were lumped into two groups only, which were the fast-reacting minerals and slow-reacting minerals based on their reactivity. In the early stage of sandstone acidizing model development, these models had been broadly applied successfully. Nevertheless, this modelling technique is insufficient to represent the acid–rock reactions when the precipitations had to be considered. The inadequacy of these models under certain condition such as high temperature resulted in the demand in improvement of the subsequent model developed by researchers. The four-parameter model, also known as the two-acid, three-mineral acidizing model was developed for the simulation of high-temperature sandstone acidizing. In this model, the precipitation reaction of amorphous silica had been taken into account of consideration. The simulation results of the model had been validated against the experimental data by Lindsay (1976)

at high-temperature condition with good agreement of the results.

In this HBF_4 acidizing simulation, the four-parameter modelling technique was adopted due to its popularity, accuracy and reliability. First, in this model, the fast-reacting minerals included the feldspar, clays and amorphous silicon as they have relatively rapid or fast reaction rate with the HF. Second, the quartz represents the slow-reacting mineral due to its relatively slow reaction rate with the HF. Finally, the silica gel is classified as the third mineral group. It is the precipitated products during the reactions.

Apart from the reactions between HF and the minerals, the reactions between fluorosilicic acid, H_2SiF_6 and the fast-reacting minerals are also included in the model. H_2SiF_6 is the product of primary reactions. During its reaction, H_2SiF_6 would react with the Al in the aluminosilicate mineral to form aluminum fluoride, AlF_3. At the same time, the Si in H_2SiF_6 will be precipitated as silica gel. This silica gel would have damaged the sandstone formation. The detail chemical reaction processes are shown in Eqs. (1)–(4) (Li et al. 2004).
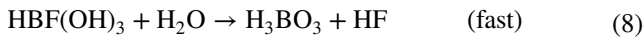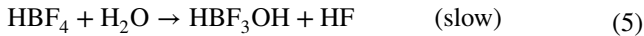
$$v_1HF + M_1 \rightarrow v_5H_2SiF_6 + AlF_3 \tag{1}$$

$$v_2HF + M_2 \rightarrow v_6H_2SiF_6 + AlF_3 \tag{2}$$

$$v_3HF + M_3 \rightarrow v_7H_2SiF_6 + AlF_3 \tag{3}$$

$$v_4H_2SiF_6 + M_1 \rightarrow v_8M_3 + AlF_3, \tag{4}$$

where v_i is the stoichiometric coefficient [1]. M_1 is the lumped group of fast-reacting minerals, representing feldspar, clays and amorphous silicon. M_2 is the lumped group of slow-reacting minerals, representing the quartz and other detrital clay. M_3 is the precipitated silica gel, $Si(OH)_4$. Some assumptions were made for these chemical reactions in the model as listed:

I. The solubility product, $K_{Si(OH)_4}^{SP}$ of silica gel, $Si(OH)_4$ is zero
II. The aluminum fluorides, AlF_3 dissolve completely in the acid solution
III. All the carbonate minerals in the core sample had dissolved completely during HCl pre-flush stage before HBF_4 main acid injection

Hydrolysis of HBF_4

In the form of aqueous solution, HBF_4 will hydrolyze step-by-step to produce HF progressively. The first step of the hydrolysis process is known as the slowest reaction, hence determining the rate of hydrolysis. Even though HF reacts with clay minerals at a very fast rate, the yield rate and the quantity of HF is limited by the hydrolysis rate and the concentration

of HBF$_4$. Theoretically, at room temperature condition, the decomposition rate of HBF$_4$ is slow, thus allowing deeper acid penetration into the rock (Zhou et al. 2016). The hydrolysis of HBF$_4$ occurs stepwise as shown in Eqs. (5)–(8).

$$HBF_4 + H_2O \rightarrow HBF_3OH + HF \qquad \text{(slow)} \qquad (5)$$

$$HBF_3OH + H_2O \rightarrow HBF_2(OH)_2 + HF \qquad \text{(fast)} \qquad (6)$$

$$HBF_2(OH)_2 + H_2O \rightarrow HBF(OH)_3 + HF \qquad \text{(fast)} \qquad (7)$$

$$HBF(OH)_3 + H_2O \rightarrow H_3BO_3 + HF \qquad \text{(fast)} \qquad (8)$$

When HF was being consumed by the sandstone minerals during the acidizing process, the equilibrium of Eqs. (5)–(8) would be shifted to the right hand side. Therefore, more HBF$_4$ would be hydrolyzed and used up to produce HF. It is clear from the equations that the penetration rate of the acid into the sandstone formation is significantly determined by the rate of HBF$_4$ decomposition. Experimental data found in the literature had proven that even though the hydrolysis rate of HBF$_4$ is first-order reaction in the concentrations of both hydrogen ion, H$^+$ and fluoroborate ion, BF$_4^-$, the overall reaction is a second-order reaction. This could be seen in the expression shown in Eq. (9).

$$r_h = k_h \times C_{H^+} \times C_{BF_4^-}, \qquad (9)$$

where r_h [mol/(m^{3}s)] is the hydrolysis rate of HBF$_4$ and k_h [m^3/mol s] is the equilibrium rate constant. C_{H^+} [mol/m^3] is the concentration of hydrogen ion, H$^+$ and $C_{BF_4^-}$ [mol/m^3] is the concentration of fluoroborate ion, BF$_4^-$.

Previous experimental studies showed that the hydrolysis rate of HBF$_4$ is a function of the temperature. Therefore, the effect of temperature must be carefully studied as it would greatly influence the sandstone acid treatment using HBF$_4$. The equilibrium constant, k_h was obtained by performing kinetic data fitting into the Arrhenius equation as shown in Eq. (10) (Zhou et al. 2016).

$$k_h = 2.4 \times 10^{15} e^{-\frac{26183}{RT}}, \qquad (10)$$

where R is the universal gas constant [cal/mol °K], T is the formation temperature [°K].

Pressure equation

The pressure distribution at each time step during the simulation must be updated to perform the prediction of acid transport in a sandstone core sample. A cubic control volume was defined in formulating the acidizing model. The acid solution used during sandstone acid core flooding process is composed of acid and water. It is assumed to comply with the law of mass conservation, which stated that in a controlled system, the mass in the closed system cannot change over time. The mass of the reactants (acid inlet) must

equal to the mass of the products (acid outlet). The pressure equation used in this model is represented by Eq. (11).

$$\frac{1}{\propto} \frac{\partial}{\partial x} \left(k_x \frac{\partial P}{\partial x} \right) + \frac{1}{\propto} \frac{\partial}{\partial y} \left(k_y \frac{\partial P}{\partial y} \right) + \frac{1}{\propto} \frac{\partial}{\partial z} \left(k_z \frac{\partial P}{\partial z} \right) = 0, \quad (11)$$

where P is the pressure [Pa].

Mass conservation of HBF$_4$

Based on the general material balance equation for acid, $i = 3$ for HBF$_4$. HBF$_4$ is a strong acid. During sandstone acidizing, HBF$_4$ underwent a complete ionization process to form H$^+$ and BF$_4^-$ in aqueous solution. So, the concentration of HBF$_4$ is the same as the concentration of its subsequent ionization product, BF$_4^-$. Hence, the hydrolysis rate of HBF$_4$ is also referred as the rate of BF$_4^-$ reduction. In a function of unit time, the change in concentration of HBF$_4$ is then equal to the net change in concentration due to both the acid fluid transport as well as the total product of hydrolysis process. Therefore, the mass balance of HBF$_4$ is shown as Eq. (12).

$$\frac{\partial (C_3 \phi)}{\partial t} + \overline{\nabla} \cdot (\bar{u} C_3) = -r_h, \qquad (12)$$

where C_3 the concentration of HBF$_4$ acid [mol/m^3], ϕ the porosity [1], $\bar{u}$ is the vector velocity [m/s]. r_h the hydrolysis rate of HBF$_4$ [mol/m^{3}s].

Mass conservation equation of acid components

The other two acid types that are involved in the sandstone acidizing process are HF ($i = 1$) and H$_2$SiF$_6$ ($i = 2$). Assuming a single-phase flow for the process and no sorption on the solid phase, in the model, the effect of dispersion can be neglected from the equation as the spread of acid front is dominantly controlled by the chemical reactions between the acids and the minerals.

For the overall acid consumption rate as well as the mineral dissolution rate, it is highly dependent on two controlling parameters. These two parameters refer to the acid flow to the surface of mineral and the true rate of reaction with the mineral surface. It is clear that the overall rate of reaction is controlled by the slower parameter. During the sandstone acid treatment, the slower process is the reaction between HF and mineral and the faster process of the transport rate of acid. Therefore, the surface reaction rate governs the overall reaction rate. During the core flooding treatment, the acid is consumed and the mass conservation equation of acid components is shown in Eq. (13).

$$\frac{\partial (C_i \phi)}{\partial t} + \overline{\nabla} \cdot (\bar{u} C_i) = -\sum_{j=1}^{N_m} E_{f,i,j} S_j^* V_j (1 - \phi) C_i^\alpha \qquad i = 1, 2, \qquad (13)$$

where C_i is the concentration of acid [mol/m³], ϕ the porosity [1], $\bar{u}$ the vector velocity [m/s], $E_{f,i,j}$ the reaction rate between the acid and mineral [m/s]. S_j^* is the reaction surface of mineral [1/m], V_j the volume fraction of mineral [1].

Mass conservation equation of minerals

The minerals in the sandstone acidizing process are dissolved and removed by two types of acid. In this model, the mass balance of the mineral species in a sandstone core matrix is represented in terms of volume fraction. Since it is assumed that only solid phase exists, all the mineral groups, j is in solid form. The change in volume of the mineral corresponds to its mass consumption divided by the density. Equation (14) shows the material balance for all the minerals involved in the sandstone acidizing reactions.

$$\frac{\partial((1-\phi)V_j)}{\partial t} = -\sum_{i=1}^{N_{a,j}} \frac{MW_i S_j^* V_j (1-\phi)\beta_{i,j} E_{f,i,j} C_i^\alpha}{\rho_j} \qquad j=1,3, \tag{14}$$

where C_i is the concentration of acid [mol/m³], ϕ the porosity [1], V_j the volume fraction of mineral [1], $N_{a,j}$ the number of acids reacting with minerals j, MW_i the molecular weight of acid i [kg/kgmol], S_j^* the reaction surface of mineral [1/m], $\beta_{i,j}$ the dissolving power of mineral j by acid i [1], $E_{f,i,j}$ the reaction rate between the acid and mineral [m/s], ρ_j the density of mineral j [kg/m³].

Change in porosity

The change in porosity during the acid core flooding process can be modelled according to the material balance of all the minerals. The porosity change in a control volume can be corresponded to the total volume of pore space being created when the minerals are being dissolved and removed. Therefore, the sum of increase in porosity per unit period of time is the total volume of each mineral dissolution deducting the volume of precipitated product generated per unit period of time. In this case, the precipitate is the silica gel. The part of the sandstone matrix that had been removed by both HF and H_2SiF_6 is included. This can be expressed as Eq. (15).

$$\frac{\partial \phi}{\partial t} = -\sum_{j=1}^{N_m}\sum_{i=1}^{N_{a,j}} \frac{MW_i S_j^* V_j \beta_{i,j} E_{f,i,j} C_i}{\rho_j}, \tag{15}$$

where ϕ the porosity [1], N_m the total number of minerals reacting with acids i, $N_{a,j}$ the number of acids reacting with minerals j, MW_t the molecular weight of acid i [g/mol], S_j^* the reaction surface of mineral [1/m], V_j the volume fraction of mineral [1], $\beta_{i,j}$ the dissolving power of mineral j by acid i [1], $E_{f,i,j}$ the reaction rate between the acid and mineral

[m/s], C_i the concentration of acid [mol/m³], ρ_j the density of mineral j [kg/m³].

Change in permeability

Apart from the display of the porosity change, the change in permeability is also one of the most important parameter that can be used to analyze the efficiency of sandstone acid treatment. Therefore, other than the chemical reaction and mechanism between the acids and the minerals, the relationship between the porosity and permeability is also a key factor that must be quantified in this model. It is commonly known that there is no single porosity–permeability relationship that can be applied to all porous formation universally.

In this simulation, the permeability enhancement is calculated at each time step and is updated based on the Labrid's equation (1975). Some of the other examples of the correlation include the Labrid's equation, Lund and Fogler's equation (1975), and Walsh and Brace's equation (1984). Nevertheless, the Labrid's equation was determined to be a suitable correlation for the relationship between the porosity and permeability for silicate sandstone. So, it is applied explicitly in each of the operation grid cell in this model. Its expression is shown in Eq. (16).

$$\frac{k_2}{k_1} = \left(\frac{\phi_2}{\phi_1}\right)^n, \tag{16}$$

where ϕ_1 is the porosity at the first time step, ϕ_2 the porosity at the second time step, k_1 the permeability at the first time step, k_2 the permeability at the second time step, $n = 3$ the coefficient correspond to the sandstone condition.

In this simulation, the pressure is calculated based on the injection rate of the acid whereas the permeability is calculated according to the Darcy's law. Hence, one can say that the pressure and permeability only depend on the porosity at a constant rate of acid injection.

Initial conditions

Before the beginning of the core flooding, it is assumed that there is no acid in the core system. Therefore, the initial conditions are shown in Eq. (17).

$$\left.\begin{aligned} C_{HBF_4} &= C_{HF} = C_{H_2SiF_6} = 0 \\ V_1 &= V_1^0 \\ V_2 &= V_2^0 \\ V_3 &= V_3^0 \\ \phi &= \phi^0 \end{aligned}\right\} \quad \text{at } t = 0, \tag{17}$$

where V_1 is the volume fraction of fast-reacting mineral [1], V_2 the volume fraction of slow-reacting mineral [1], V_3 the volume fraction of silica gel precipitate [1], V_1^0 original volume fraction of fast-reacting mineral [1], V_2^0 original volume fraction of slow-reacting mineral [1], ϕ^0 original porosity of the core sample [1].

Boundary conditions

The acid core flooding process occurs such that the acid is constantly being injected from the left side into the inlet face of the sandstone core at a fixed injection rate. However, when the porosity and permeability is updated during the simulation, the rate of acid injection in each mesh would also change with respect to time. This means that this boundary condition is not directly applicable in the model. Hence, this issue is solved by assigning a guess to the initial pressure values, P_0. So, the model equations would be computed and calculated based on the initial inlet pressure being input. As soon as updating the pressure change, the rate of acid injection at each mesh would be calculated based on the Darcy's law in the model. This calculated rate of injection would then be compared against the input value, thus adjusting the initial pressure. The value of subsequent P_0 is predicted according to the difference between the calculated injection rate and the input injection rate as well as the latest P_0 value updated. The iteration process would continue until successful data convergence and the correct initial pressure are obtained.

The concentration of acid at the inlet face of the core sample equals to the concentration of acid injected, C_i^0. Then, the acid exits from the right side of the core sample, which is the outlet face. A constant pressure is exerted at the outlet of the core. So, there is only one-dimensional flow of acid across the two ends of the core sample. For the curve or circular side of the cylindrical core plug, it is assumed that there is no flow on that boundary. Thus, the boundary condition of the model is expressed as Eqs. (18)–(20).

$$\left. \begin{array}{l} C_{HF} = C_i^0 \\[1em] P = P_0 \\[1em] Q = \text{Constant} \end{array} \right\} \qquad \text{at } x = 0 \qquad (18)$$

$$P = P_{out} \qquad \text{at } x = L \qquad (19)$$

$$\frac{\partial P}{\partial r} = 0 \qquad \text{at } r = r_c, \qquad (20)$$

where Q is the injection rate of acid [m/s], P_{out} back pressure exerted at the outlet face of the core [Pa], L length of core sample [in], r_c radius of core sample [in].

Summary of governing equations

Finally, all the necessary equations as well as initial and boundary conditions that had been adopted in this model to describe the sandstone acidizing process are summarized in this section. It includes the key equations used to solve the pressure field, concentration of acids and concentration of minerals.

$$\frac{1}{\propto} \frac{\partial}{\partial x} \left(k_x \frac{\partial P}{\partial x} \right) + \frac{1}{\propto} \frac{\partial}{\partial y} \left(k_y \frac{\partial P}{\partial y} \right) + \frac{1}{\propto} \frac{\partial}{\partial z} \left(k_z \frac{\partial P}{\partial z} \right) = 0 \qquad (11)$$

$$\frac{\partial (C_3 \phi)}{\partial t} + \overline{\nabla} \cdot (\bar{u} C_3) = -r_h \qquad (12)$$

$$\frac{\partial (C_i \phi)}{\partial t} + \overline{\nabla} \cdot (\bar{u} C_i) = -\sum_{j=1}^{N_m} E_{f,i,j} S_j^* V_j (1 - \phi) C_i^\alpha \qquad i = 1, 2 \qquad (13)$$

$$\frac{\partial ((1 - \phi) V_j)}{\partial t} = -\sum_{i=1}^{N_{a,j}} \frac{MW_i S_j^* V_j (1 - \phi) \beta_{i,j} E_{f,i,j} C_i^\alpha}{\rho_j} \qquad j = 1, 2, 3 \qquad (14)$$

$$\frac{\partial \phi}{\partial t} = -\sum_{j=1}^{N_m} \sum_{i=1}^{N_{a,j}} \frac{MW_i S_j^* V_j \beta_{i,j} E_{f,i,j} C_i}{\rho_j} \qquad (15)$$

$$\frac{k_2}{k_1} = \left(\frac{\phi_2}{\phi_1} \right)^n \qquad (16)$$

$$\left. \begin{array}{l} C_{HBF_4} = C_{HF} = C_{H_2SiF_6} = 0 \\[1em] V_1 = V_1^0 \\[1em] V_2 = V_2^0 \\[1em] V_3 = V_3^0 \\[1em] \phi = \phi^0 \end{array} \right\} \qquad \text{at } t = 0 \qquad (17)$$

$$\left. \begin{array}{l} C_{HF} = C_i^0 \\[1em] Q = \text{Constant} \end{array} \right\} \qquad \text{at } x = 0 \qquad (18)$$

$$P = P_{out} \qquad at\ x = L \qquad\qquad (19)$$

$$\frac{\partial P}{\partial r} = 0 \qquad at\ r = r_c \qquad\qquad (20)$$

Numerical solution and implementation of the model

For further investigation of sandstone acidizing process using modelling approach, COMSOL® Multiphysics commercial software of Computational Fluid Dynamics (CFD) is suggested to be used in the development of core flooding model using finite element method (FEM). COMSOL® is sophisticated and convenient tool that is able to perform detailed 3D geometric modelling and simulation. All the model parts, the process parameters and also the simulation control including the boundary conditions and mesh control can be defined in several stages. In general, the following steps should be considered to develop a simulator.

Geometry creation

The geometry created is a cylindrical-shaped sandstone core plug. The dimension of the geometry is 3 inch long with 1.5 inch diameter. This geometry is simulating a typical sandstone core sample that is commonly used during the core flooding experiments. It is being generated directly in the COMSOL® software by key in the radius and length in the domain interface. Then, the object type is selected as solid, simulating a generalized homogeneous Berea sandstone core.

Grid blocks creation and mesh independence analysis

Prior to proceeding with the real numerical simulation and model verification, the mesh independence analysis was conducted. In ideal case, the accuracy of the simulation results obtained is higher when the mesh size is finer and the domain element is denser. At the same time, it must be understood that the period of computational time to complete the simulation run would also be longer. This is due to the significantly increased calculation workload and solving of the governing equations in the model at each time step.

However, at a certain point of mesh size increased, the accuracy of the simulation data becomes insignificant and can be neglected. Hence, selecting an optimum mesh size based on the accuracy of simulation result while taking the computational time into consideration is crucial in a modelling study. It is also a typical procedure for any kind of CFD modelling study.

In present work, the mesh independency was checked to obtain a threshold grid size of the geometry, where the further grid size refinement would only cause ignorable effect on the simulation data. The optimum grid size selected would then be used to simulate all the simulation cases while providing optimum accuracy. A total of four different mesh sizes had been used for mesh independence analysis and the results of porosity, permeability and pressure after numerical simulation were exported. These include the normal, fine, finer and extra-fine meshes. A physics-controlled mesh sequence type was selected while building the mesh.

To select the optimum grid size, the porosity profile was observed. The mesh independency analysis results were obtained. Judging from the porosity profiles, it is clearly observed that the porosity increment due to different mesh size is not significantly altered.
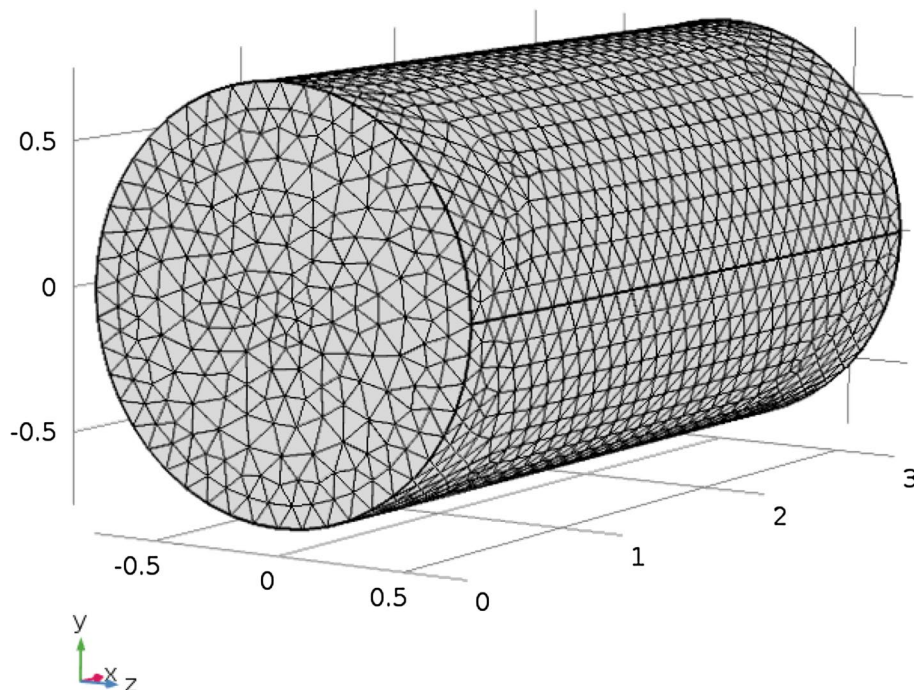
Based on the final porosity, permeability and pressure extracted, it is demonstrated that nearly constant values are achieved from normal mesh to extra-fine mesh. Therefore, further reduction in the grid size of the geometry is not a necessary step since it does not influence the accuracy of the results. Nevertheless, since the computational time for one run of simulation using the extra-fine mesh size is within 30 min and is acceptable for this study, the final mesh size selected is the extra-fine mesh. This would ensure a more accurate result obtained in the subsequent parametric study or sensitivity analysis.

Figure 1 shows the schematic diagram for the meshing of the cylindrical sandstone core by selecting the extra-fine element size. Referring to the axis orientation, the x-axis corresponds to the main direction of acid transport whereas the y-axis and z-axis represented the cross-sectional plane of the core where it is assumed there is no flow across them. So, the final mesh is made up of 77,516 domain elements, 4068 triangular elements, 212 edge elements and 8 vertex elements. The simulation time required to complete each run is approximately 26 min. Once the mesh independency is secured, then the subsequent simulations could be run without major concern in relation to the grid size.

Model input and setting

Table 1 provides all the required input parameter and necessary coefficients for the simulation. In the numerical simulation, the geometry of the core sample is designed to be the same as the experimentally used core sample in the literature, which is cylindrical-shaped. The dimension of the core sample is set as 3 in long and 1.5 in diameter. This core plug was run throughout all the simulations. The initial porosity and permeability of the core sample were also set based on the experimental condition, which are 12% and 40 mD, respectively. In this model, the initial porosity and permeability of the core sample were kept constant along the

Fig. 1 The meshing of the geometry using extra-fine element size

core plug. Hence, the transport mechanism of the model was simplified to only one-dimensional flow, which is only in the direction from the inlet face to the outlet face (x-direction).

For the simulation condition, acid is being injected at constant injection velocity of 2.23×10^{-5} m/s. The temperature condition is set as 25 °C in the first simulation. However, this is a subjective parameter that can be varied and changed later on for parametric study. The reference pressure level and outlet pressure were set as 14.7 psi (101,325 Pa) and 1 psi (6894.76 Pa), respectively. Whereas the time step of the simulation was input at 5 min. It is the time interval between two time steps. Therefore, data of the results generated during the simulation were recorded every 5 min until the simulation stopped.

The values of reaction rate constant, dissolving power and stoichiometry coefficient listed in Table 1 were determined from the literature data provided by Da Motta et al. (1993). The values are the Damkohler numbers that had been used in fitting the test data by Lindsay (1976). Different chemical reaction between acids and minerals would have different values of reaction rate constant and dissolving power. Four main acid and mineral reactions occurring during the core flooding were considered in this model, which included the reactions between HF and fast-reacting minerals, HF and slow-reacting minerals, HF and silica gel, as well as H_2SiF_6 and fast-reacting minerals. Their respective reaction rate constants are 0.127, 2.32×10^{-8}, 2×10^{-7} and 5×10^{-5} m/s. Their mass dissolving powers are 0.486, 0.5, 0.8 and 2.47, respectively. These reaction rate constants and dissolving powers were well understood and could be determined from

the literatures (Economides et al. 2013). The stoichiometry coefficients of the four main reactions $v_1 - v_8$ are 27, 6, 6, 1, 3, 1, 1 and 2.5, respectively (Da Motta et al. 1993).

Other information regarding the acids and minerals is listed in Table 1. The main injected acid is HBF_4. After being hydrolyzed, it will produce HF, which is the reacting acid. There are two reacting acids and three reacting minerals in the model. The two reacting acids are HF and H_2SiF_6 whereas the three reacting minerals are fast-reacting mineral, slow-reacting mineral and silica gel (carbonates precipitate). The basic acid information required is the acid viscosity (8.9×10^{-4} Pa s), acid density (1075 kg/m^3), acid diffusion coefficient (1×10^{-6} m^2/s) and acid concentration (1469 mol/m^3). The value of the acid concentration is based on 12% HBF_4 used. The relative molecular weights of HF and H_2SiF_6 are 20 and 144 g/mol respectively.

For the mineral information required in the model, the relative molecular weights of fast-reacting minerals, slow-reacting minerals and silica gel are 262, 60 and 96 g/mol, respectively. The volume fraction of fast-reacting minerals, slow-reacting minerals and silica gel were set to be 0.20, 0.78 and 0.02. These values are the same as the experimentally used core sample. Different core sample used might have different volume fraction of minerals. The sum of the volume fraction of the three mineral groups is 1. Furthermore, the specific reaction surface areas of fast-reacting minerals, slow-reacting minerals and silica gel are 235,000, 300,000 and 330,000 m^{-1}. Last but not least, the last group of parameters input in the model is the density. The densities

Table 1 Required input parameter in the model

Parameter	Value	Unit	Parameter	Value	Unit
(a) Core information			(b) Kinetic parameter		
Core length, l	3	in	Reaction rate constant of HF and fast-reacting minerals	0.127	m/s
Core diameter, D	1.5	in	Reaction rate constant of HF and slow-reacting minerals	2.32×10^{-8}	m/s
Initial porosity, ϕ	0.12	[1]	Reaction rate constant of HF and silica gel	2×10^{-7}	m/s
Initial permeability, k	40	mD	Reaction rate constant of H_2SiF_6 and fast-reacting minerals	5×10^{-5}	m/s
(c) Simulation condition			(d) Acid information		
Injection velocity, v	2.23×10^{-5}	m/s	Acid viscosity, μ	8.9×10^{-4}	Pa s
Time step, t	5	min	Acid density, ρ_{acid}	1075	kg/m³
Temperature, T	25	°C	Acid diffusion coefficient, D_c	1×10^{-6}	m²/s
Reference pressure level, P_{ref}	101,325	Pa	Acid concentration, C_{acid}	1469	mol/m³
Outlet pressure, P_{out}	6894.76	Pa	Relative molecular weight of HF	20	g/mol
(e) Mass dissolving power			Relative molecular weight of H_2SiF_6	144	g/mol
Mass dissolving power of HF and fast-reacting minerals	0.486	[1]	(f) Mineral information		
Mass dissolving power of HF and slow-reacting minerals	0.5	[1]	Relative molecular weight of fast-reacting minerals	262	g/mol
Mass dissolving power of HF and silica gel	0.8	[1]	Relative molecular weight of slow-reacting minerals	60	g/mol
Mass dissolving power of H_2SiF_6 and fast-reacting minerals	2.47	[1]	Relative molecular weight of silica gel	96	g/mol
(g) Stoichiometry coefficients			Volume fraction of fast-reacting minerals	0.20	[1]
v_1	27	[1]	Volume fraction of slow-reacting minerals	0.78	[1]
v_2	6	[1]	Volume fraction of silica gel	0.02	[1]
v_3	6	[1]	Specific reaction surface area of fast-reacting minerals	235,000	1/m
v_4	1	[1]	Specific reaction surface area of slow-reacting minerals	300,000	1/m
v_5	3	[1]	Specific reaction surface area of silica gel	330,000	1/m
v_6	1	[1]	Density of fast-reacting minerals	2600	kg/m³
v_7	1	[1]	Density of slow-reacting minerals	2650	kg/m³
v_8	2.5	[1]	Density of silica gel	740	kg/m³

of fast-reacting minerals, slow-reacting minerals and silica gel are 2600, 2650 and 740 kg/m³.

Numerical visualization, simulation results and discussion

Model validation

After modelling all the governing equations describing the sandstone acidizing process, HBF$_4$ acidizing is simulated in the COMSOL® Multiphysics commercial software. Prior to conduct further simulation investigation at higher temperature as well as performing design optimization study on various parameters affecting the sandstone acidizing process using HBF$_4$ acid, it is crucial to validate the feasibility of

the model. This is very important so that the results obtained from this simulation study would be verified. Hence, the HBF$_4$ simulation results at 25 and 65 °C were being validated against the experimental data obtained from the literature by Zhou et al. (2016).

Figures 2 and 3 show the plot of the comparison between HBF$_4$ acidizing simulation result and experimental data at 25 and 65 °C, respectively. The plot of permeability ratio, k/k_0 versus time of main acid injection is obtained. The results showed that the simulation results have fairly good agreement with the experimental results. The high consistency of the simulation results fitting the experimental data indicates that the model is reliable for further investigation.

From Figs. 2 and 3, it is clear that the fluoroboric acidizing treatment at 25 °C resulted in permeability enhancement ratio of only 1.2 along the core plug after 35 min,

Comparison of Fluoroboric Acidizing Simulation Result and Experimental Data at 25 °C
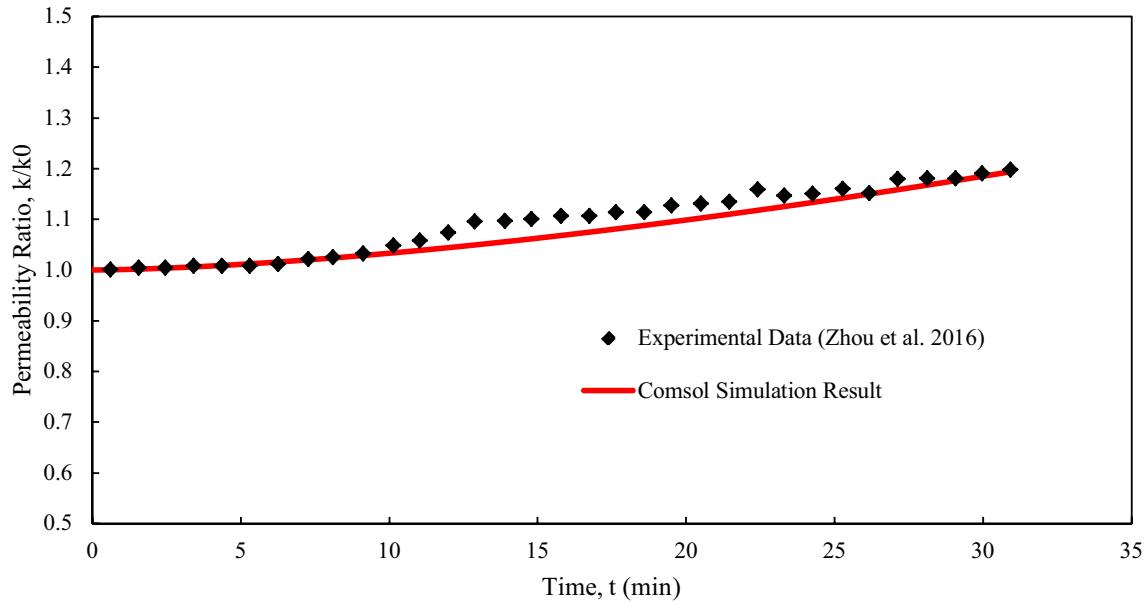

Fig. 2 Plot of comparison between fluoroboric acidizing simulation result and experimental data at 25 °C

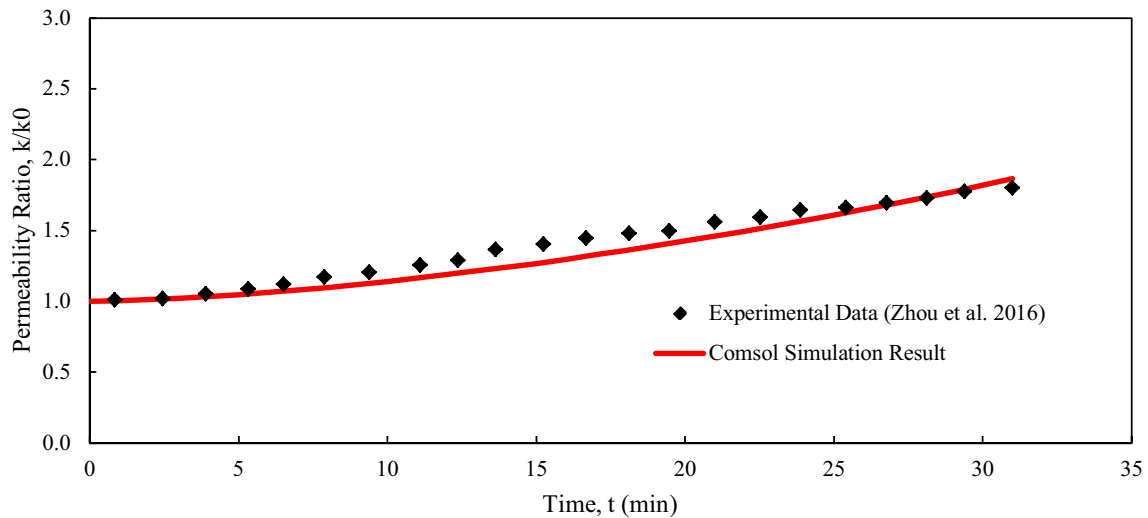## Comparison of Fluoroboric Acidizing Simulation Result and Experimental Data at 65 °C

Fig. 3 Plot of comparison between fluoroboric acidizing simulation result and experimental data at 65 °C

which is nearly no improvement and not significant. However, at increased temperature of 65 °C, the permeability ratio enhancement after 35 min is drastically increased to approximately 1.9. The improved permeability to initial permeability of the core sample is almost doubled, which demonstrated significant result.

Fig. 4 Porosity distribution after 25 min (left) and after 35 min (right) of fluoroboric acid injection at **a** 25 °C, **b** 65 °C and **c** 105 °C

Effect of temperature

Results and discussion on porosity and permeability distribution

When the temperature increases, the hydrolysis rate of HBF_4 also increases. The chemical reaction shifts to the right, producing more HF. Therefore, the hydrolysis rate of HBF_4 acts as the governing factor, controlling the chemical reaction and mechanism between the HBF_4 acid and the sandstone minerals. Therefore, it is known that the porosity and permeability improvement of the sandstone core is eventually affected by the formation temperature condition.

Fig. 5 Permeability distribution after 25 min (left) and after 35 min (right) of fluoroboric acid injection at **a** 25 °C, **b** 65 °C and **c** 105 °C

In this study, HBF$_4$ acidizing treatment was simulated at a wide range of temperature, including 25, 45, 65, 85 and 105 °C. In this numerical simulation, all the main parameters are set according to the experimental condition. The

Table 2 Effect of temperature on porosity enhancement ratio

Temperature, T (°C)	Initial porosity, ϕ_0	Final porosity, ϕ_f	Porosity enhancement ratio, ϕ_f/ϕ_0
25	0.12	0.1286	1.07
45	0.12	0.1369	1.14
65	0.12	0.1507	1.26
85	0.12	0.1713	1.43
105	0.12	0.2004	1.67

Table 3 Effect of temperature on permeability enhancement ratio

Temperature, T (°C)	Initial permeability, k_0(m^2) ($\times 10^{-14}$)	Final permeability, k_f (m^2)	Permeability enhancement ratio, k_f/k_0
25	3.95	4.87E−14	1.23
45	3.95	5.91E−14	1.50
65	3.95	8.12E−14	2.06
85	3.95	1.31E−13	3.32
105	3.95	2.79E−13	7.06

acid used is 12% HBF$_4$ combined with 12% HCl, and is being injected at a constant rate of 2.23×10^{-5} m/s. The initial porosity and permeability are set to be 12% and 3.95×10^{-14} m^2, respectively.

The HBF$_4$ acid is being injected from the left side or the inlet face and breakthrough from the right side or the outlet face of the core plug. When the acid is injected into the core, the acid would begin to react and the minerals present in the rock are being dissolved and removed, hence increasing the sandstone core porosity and permeability.

The low-, medium- and high-formation temperature conditions are represented by 25, 65, and 105 °C, respectively. After 5, 15, 25, and 35 min of the fluoroboric acid injection, the results of the 3D numerical visualization are obtained. However, only the results after 25 and 35 min were shown here in this paper. The porosity and permeability distribution of the core at 25, 65, and 105 °C due to acid dissolution and precipitation reactions are shown in Figs. 4 and 5, respectively. This simulation is based on homogeneous sandstone condition, therefore, the moving of injected acid at the front end of the core plug is observed to be uniform throughout the length of the core plug. There is no preferential flow path being created along the core sample as the porosity and permeability distribution being decreased in a gradual and uniform pattern from the entering side until the exiting end of the core geometry.

Fig. 6 The effect of temperatures on sandstone porosity after fluoroboric acidizing

Permeability versus Time of Acid Injection at Different Temperatures
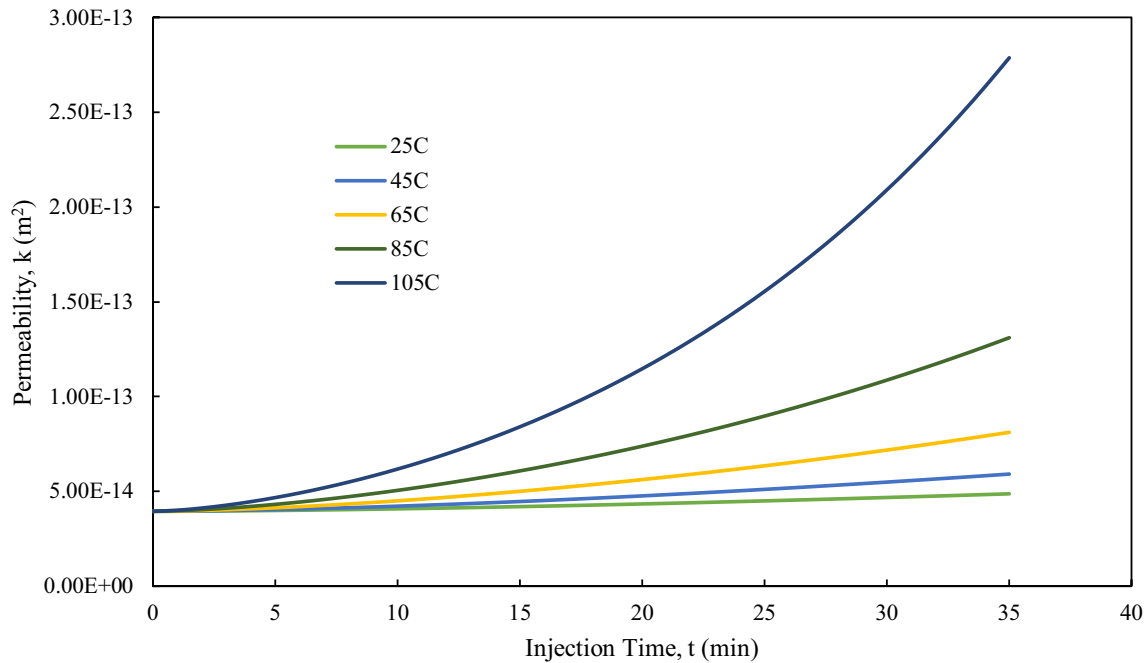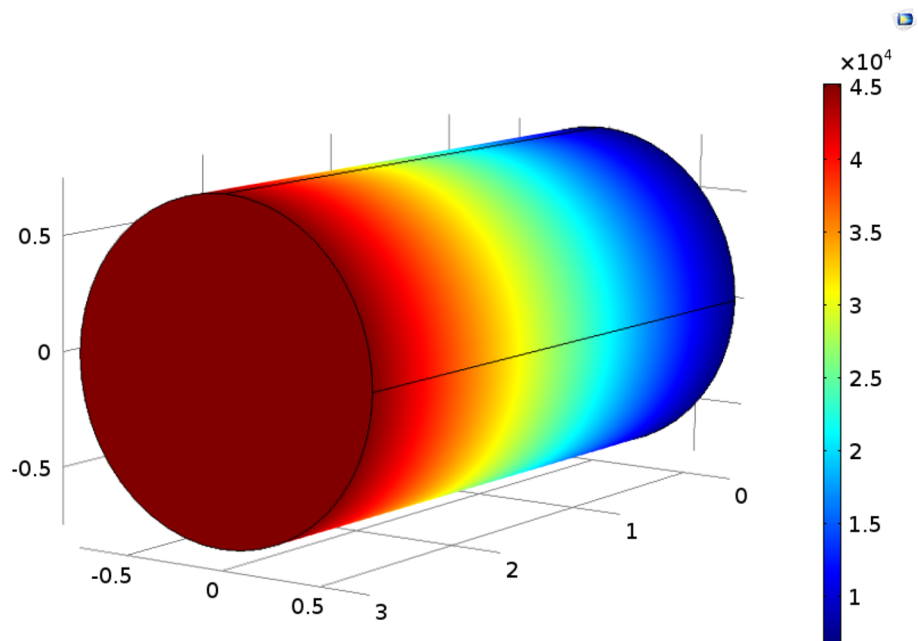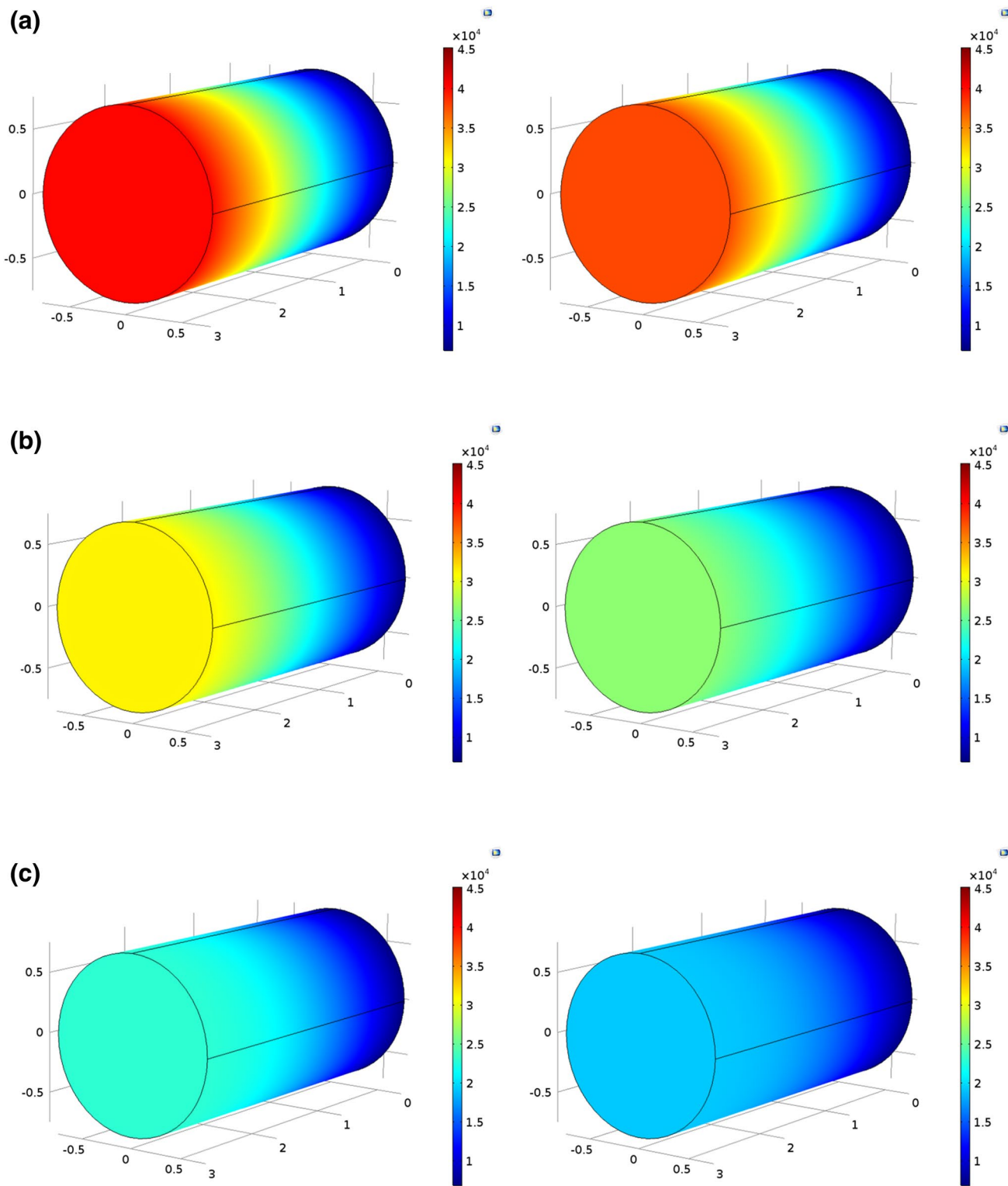

Fig. 7 The effect of temperatures on sandstone permeability after fluoroboric acidizing

Fig. 8 Initial pressure distribution at the beginning of acid injection

Based on the simulation results, the injection of HBF_4 has successfully increased the porosity to 0.1286; and permeability to 4.87×10^{-14} m^2. This demonstrated that even at room temperature of 25 °C, porosity and permeability enhancement were observed in the sandstone core, with the porosity and permeability increase of 1.07 times and 1.23 times the initial value, respectively. The performance of HBF_4 acid is a function of the temperature. It highly depends on the effect of temperature. The permeability increase is not significant enough due to the slow hydrolysis rate of the HBF_4 acid at room temperature, which limited the speed of acid spending.

Nevertheless, when the temperature is increased to 65 °C, the hydrolysis rate of HBF_4 increases significantly, hence increasing the porosity and permeability enhancement ratio.

Fig. 9 Pressure distribution after 25 min (left) and after 35 min (right) of fluoroboric acid injection at **a** 25 °C, **b** 65 °C and **c** 105 °C

Hence, the gradient of the permeability enhancement is also significantly improved. At 65 °C, the porosity of the sandstone core increases to 0.1507, with porosity enhancement ratio of 1.26 times. Whereas for the permeability, an increment to 8.12×10^{-14} m^2 is obtained, with permeability enhancement ratio of 2.06 times.

Table 4 Effect of temperature on pressure drop

Temperature, T (°C)	Initial pressure, P_0 (Pa)	Final pressure, P_f (Pa)	Pressure Drop, ΔP (Pa)
25	26039.68168	22965.60533	3074.076347
45	26040.40886	20778.51802	5261.890847
65	26041.84560	18267.21372	7774.631886
85	26044.60449	16268.37189	9776.232603
105	26049.89308	15354.20302	10695.69005

Meanwhile at 105 °C, which better represents the real high temperature field condition, the HBF_4 acid treatment successfully increases the porosity to 0.2004 and permeability to 2.79×10^{-14} m^2, with their respective porosity and permeability enhancement ratio of 1.67 and 7.06 times. This had proven that at high temperature condition, the acid and rock reactions became more drastic as more HF is being produced from the hydrolysis reaction.

As seen in Figs. 4 and 5, it is observed that generally the sandstone core zone that had been dissolved by the acid injected is the one-third region of the core length. In other word, most of the acid is being consumed effectively around the inlet face of the core, with porosity and permeability distribution decreases gradually. Also, the slow hydrolysis process of HBF_4 allowed deep penetration into the core. Therefore, a gentle porosity and permeability profile is obtained.

The complete results of simulation based on the five temperatures at 25, 45, 65, 85 and 105 °C are tabulated in Tables 2 and 3. The initial and final porosity and permeability as well as their respective porosity and permeability enhancement ratios are shown in the Tables. The graph of porosity and permeability are plotted against the time of acid injection as in Figs. 6 and 7. Generally, it can be seen that the porosity and permeability increases when the formation temperature becomes higher. This is due to higher rate of hydrolysis and the reactivity of acid at higher temperature.

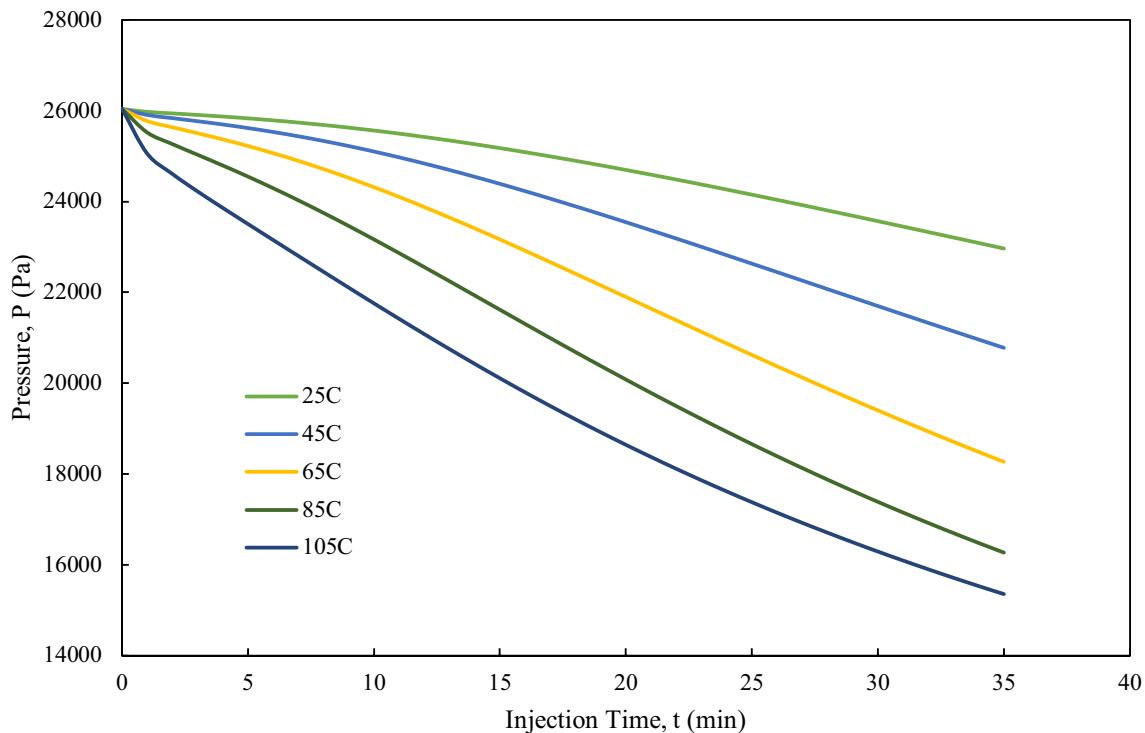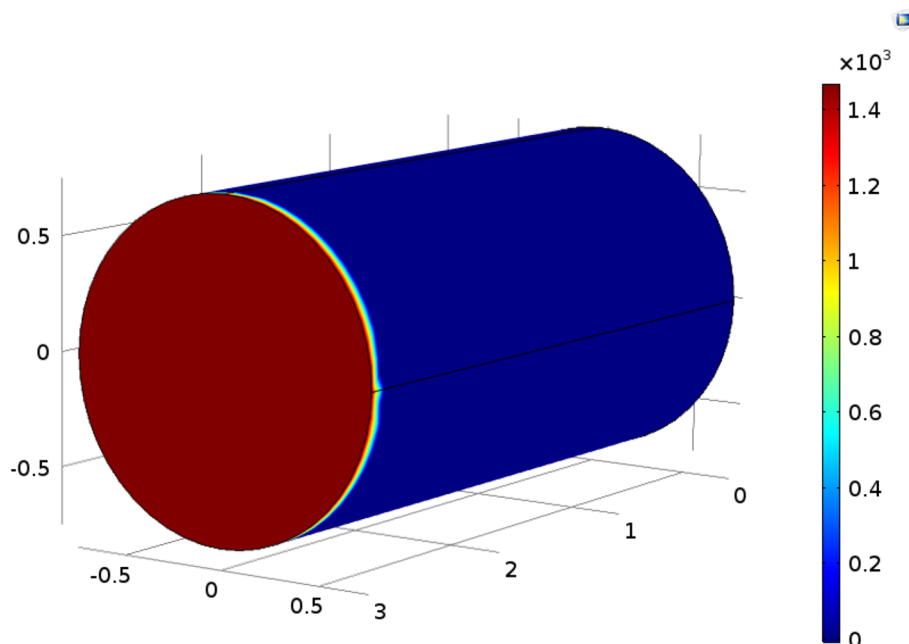Pressure versus Time of Acid Injection at Different Temperatures

Fig. 10 The effect of temperatures on sandstone pressure drop after fluoroboric acidizing

Fig. 11 Initial HBF$_4$ acid distribution at the beginning of acid injection

Results and discussion on pressure and acids concentration distribution

Figure 8 shows the initial pressure distribution in the sandstone core when the acid injection process begin. After the acid treatment process, the pressure drop occurs. The pressure distribution in the sandstone core plug after 25 min and after 35 min of acid injection was obtained and is shown in Fig. 9. Based on the 3D visualization result, it is observed that the pressure drop at 25 °C is not so obvious. However, at higher temperatures of 65 and 105 °C, the pressure drops significantly due to more acid consumption and mineral dissolution. Due to increased hydrolysis rate, the chemical reaction between the acids and the minerals becomes more active, hence resulting in higher difference in pressure drop.

The complete pressure drop results of simulation based on the five temperatures at 25, 45, 65, 85 and 105 °C are tabulated in Table 4. The initial and final pressure and the pressure drop rates are shown in the Table. Figure 10 illustrated the pressure drop curve for the HBF$_4$ acid treatment process at different temperatures generated during the simulation. The acidizing treatment resulted in pressure reduction in a gradual pattern along the core flooding process. Based on the pressure response curve, it is clear that when the temperature increases, the pressure drop is more drastic due to the rapid hydrolysis reaction and acid–rock reaction.

Figure 11 shows the initial HBF$_4$ acid distribution in the sandstone core at the beginning of the acid core flooding process. From the figure, it is clear that the acid is distributed uniformly along the core, starting from the inlet face of the core. Then, slowly along the core flooding process,

the HBF$_4$ acid distribution along the sandstone core sample after 25 min and 35 min of acid injection is shown in Fig. 12. From the figure, the HBF$_4$ acid penetrated more evenly and slowly along the sandstone core length at 25 °C because the hydrolysis rate is slow. At 65 °C, the hydrolysis rate increases and the reduction of HBF$_4$ acid concentration becomes faster. Whereas at even higher temperature of 105 °C, most of the HBF$_4$ acid is spent at the region near the inlet face of acid injection. This is due to very high hydrolysis rate and acid spending speed.

Meanwhile, from Fig. 12, it is noticeable that the acid front penetrated more than one-third of the core region. This scenario had proven that the chemical reactions between the acid and rock resulted in more acid front spreading or penetration into the core as compared to the effect of dispersion. Therefore, it is valid and reasonable to assume there is no dispersion in this study.

The full results of initial and final HBF$_4$ concentration after acid core flooding simulation at the five temperatures of 25, 45, 65, 85 and 105 °C are tabulated in Table 5. The higher the temperature, the lower the final HBF$_4$ concentration because of the increased rate of hydrolysis, which causes more acid consumption.

Figure 13 illustrates the HBF$_4$ concentration curve during acid treatment process at different temperatures generated. In general, the curve pattern of the concentration of HBF$_4$ along the core flooding process showed a sharp increment at the beginning of the acid injection. Then, it continues to increase progressively until it reached the equilibrium concentration, which eventually leads to a nearly constant concentration value. Based on the HBF$_4$ concentration curve, it
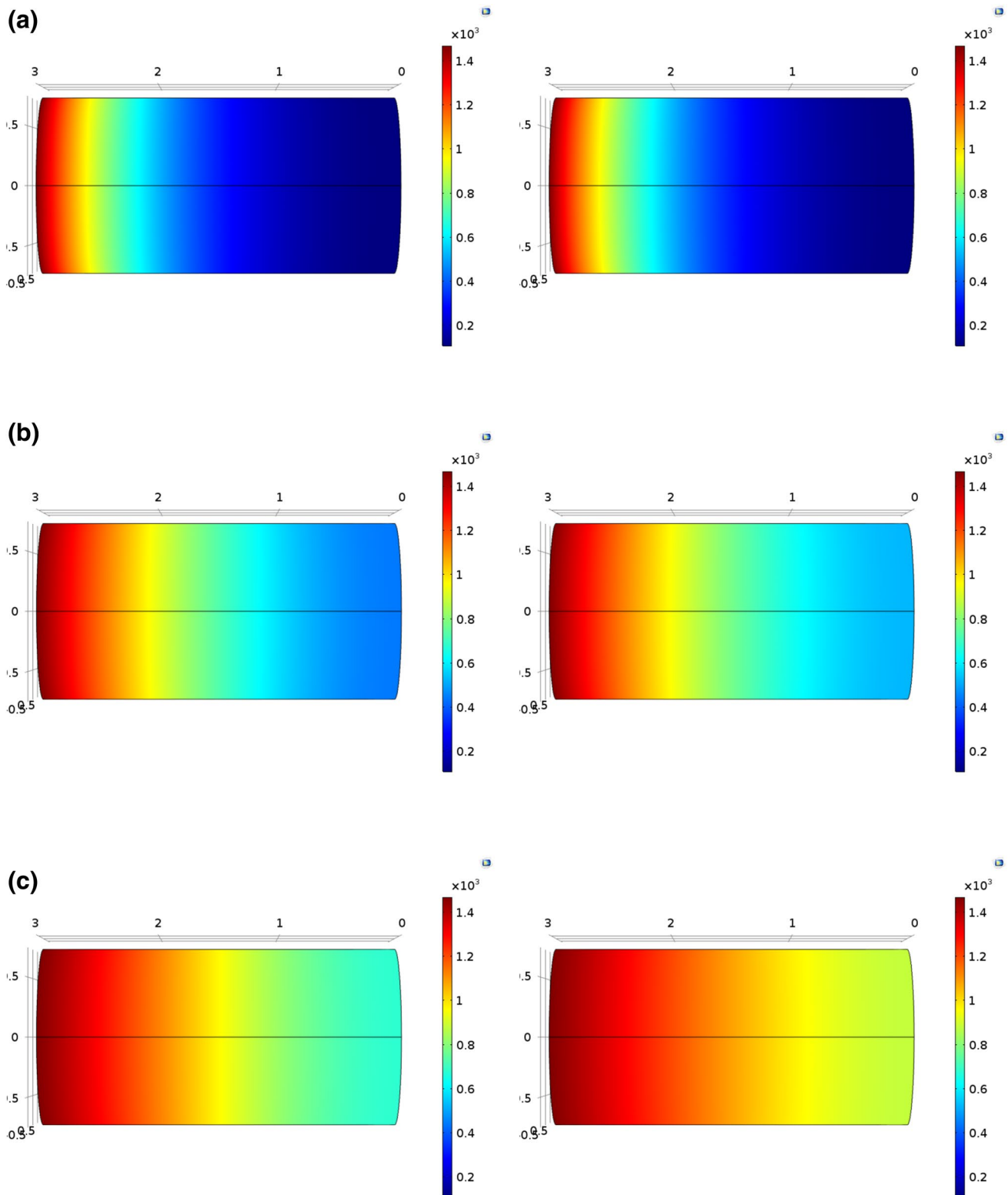
Fig. 12 HBF$_4$ acid distribution after 25 min (left) and after 35 min (right) of fluoroboric acid injection at **a** 25 °C, **b** 65 °C and **c** 105 °C

indicates that effective acidizing occur as soon as the acid begins to be injected and slowly weaken. Furthermore, when the temperature increases, it is noticeable that the HBF$_4$ would be spent more quickly, and therefore, reaching an equilibrium constant sooner. This is also attributed to the rapid hydrolysis reaction.

Table 5 Effect of temperature on HBF$_4$ concentration

Temperature, T (°C)	Initial HBF$_4$ concentration (mol/m^3) ($\times 10^1$)	Final HBF$_4$ concentration (mol/m^3)
25	1.69	1.11E+03
45	1.69	1.01E+03
65	1.69	8.48E+02
85	1.69	6.51E+02
105	1.69	4.62E+02

Table 6 Effect of temperature on HF concentration

Temperature, T (°C)	Initial HF concentration (mol/m^3)	Final HF concentration (mol/m^3)
25	5.01E−07	3.36E−05
45	1.04E−06	6.58E−05
65	2.11E−06	1.21E−04
85	4.16E−06	2.15E−04
105	8.09E−06	4.76E−04

Referring to Table 5, the initial HBF$_4$ concentration at all the temperature ranges are the same, which is 1.69×10^1 mol/m^3. This is the acid concentration calculated as soon as the core flooding process begins. Its initial value depends on the initial injected value. However, it is not the same case for HF and H$_2$SiF$_6$ concentrations. Tables 6 and 7 show the results of HF and H$_2$SiF$_6$ concentration, respectively, at different temperatures. It could be seen that the initial values for HF and H$_2$SiF$_6$ are different for varied temperature conditions. This is because their initial and final concentrations depend on the hydrolysis rate of HBF$_4$ and subsequent chemical

Table 7 Effect of temperature on H$_2$SiF$_6$ concentration

Temperature, T (°C)	Initial H$_2$SiF$_6$ Concentration (mol/m^3)	Final H$_2$SiF$_6$ Concentration (mol/m^3)
25	1.24E−06	9.49E−03
45	2.58E−06	1.86E−02
65	5.22E−06	3.41E−02
85	1.03E−05	6.06E−02
105	2.00E−05	1.33E−01

Fig. 13 The effect of temperatures on HBF$_4$ concentration along acid injection time

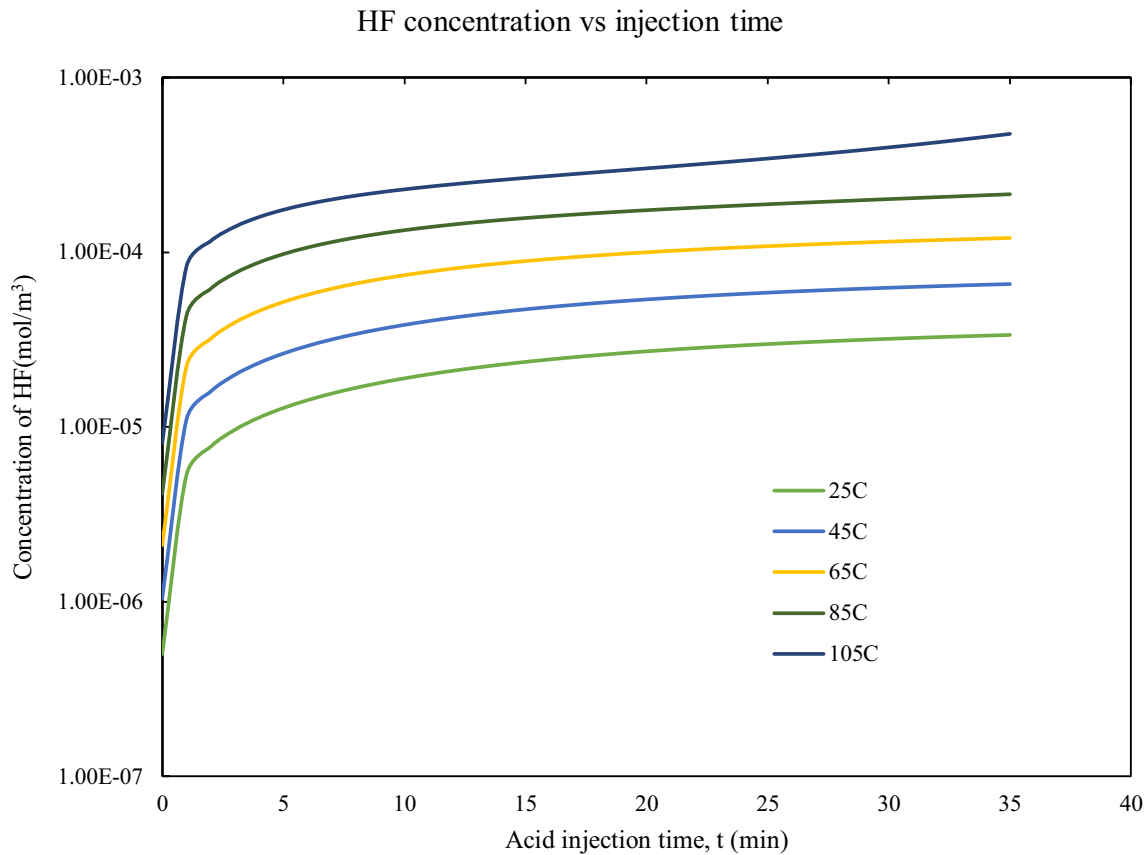## HF concentration vs injection time

Fig. 14 The effect of temperatures on HF concentration along acid injection time

reactions, which are strongly affected by the temperature parameter.

In plot form, the respective HF and H_2SiF_6 concentration curves are graphically shown in Figs. 14 and 15. Overall, the concentration of HF would increase simultaneously with the consumption of HBF_4 main acid through hydrolysis process. On the other hand, the concentration of H_2SiF_6 would increase synchronously with the consumption of HF acid through the chemical reaction with the sandstone minerals during acid treatment. At increased temperature environments, the rate of hydrolysis rate would increase. Hence, this would also lead to increase in subsequent HF and H_2SiF_6 concentration reasonably.

Results and discussion on mineral's volume fraction distribution

In this simulation, the acid spreads gradually along the core sample. By 35 min, acid had been injected into the core, the simulation process stop converging and end the simulation.

This is an indication that the effluent acid begins to be produced from the outlet face of the core at that point of time. For the homogeneous case, the time of acid breakthrough is 35 min.

Apart from the mineral dissolution of the fast-reacting and slow-reacting minerals, there is also a zone of precipitation reaction, resulting the formation of the precipitated products, which is the silica gel, $Si(OH)_4$. In present study, it is observed that the variation in the volume fraction of slow-reacting mineral is not significant at low temperature of 25 °C. There is only subtle change in quartz concentration contributed in the simulation. Hence, this is a clear indication that the chemical reaction the acid with the slow-reacting minerals is not helpful in porosity and permeability enhancement. Similar results were observed at increased temperature conditions of 45, 65, 85 and 105 °C. Thus, the results for slow-reacting mineral volume fraction are excluded in this section since their reaction with the acid is not significant and could be neglected.
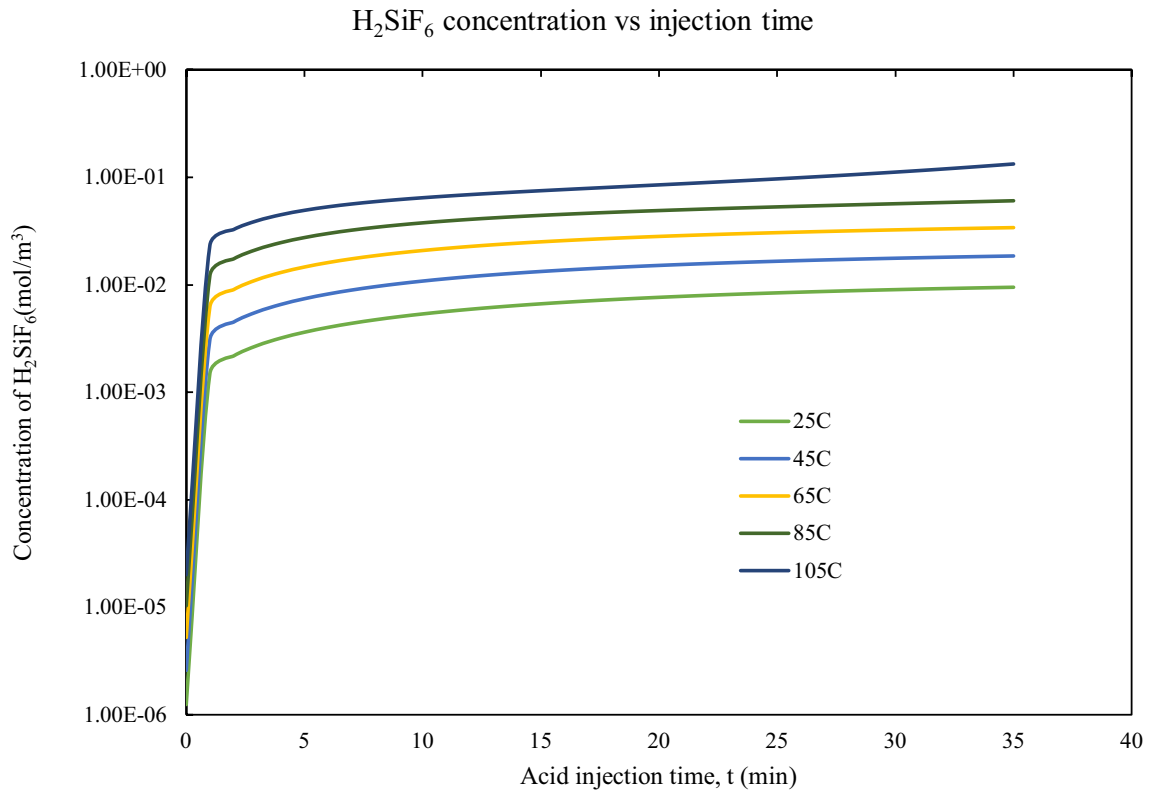
H_2SiF_6 concentration vs injection time

Fig. 15 The effect of temperatures on H_2SiF_6 concentration along acid injection time

Fig. 16 Initial fast-reacting mineral distribution at the beginning of acid injection
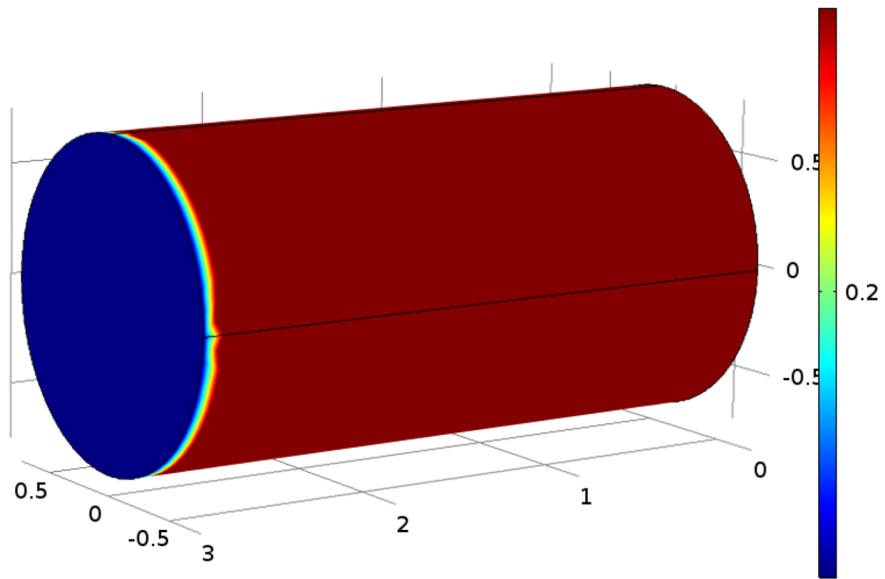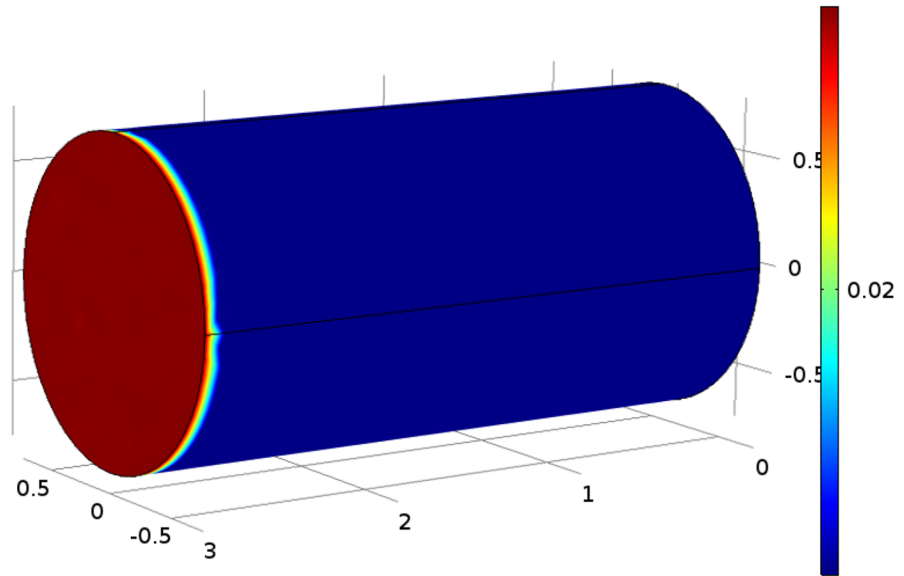
Fig. 17 Initial silica gel precipitate distribution at the beginning of acid injection

Figures 16 and 17 show the initial fast-reacting mineral and silica gel precipitate distribution in the sandstone core once the acid core flooding process started. From Fig. 16, the fast-reacting mineral would begin to decrease as it is being consumed in the acid–rock chemical reaction. On the other hand, the silica gel precipitate would begin to increase as it is being produced in the acid–rock chemical reaction as demonstrated in Fig. 17. After 35 min of HBF_4 acid injection, the distribution of both this minerals inside the core plug at 25, 65 and 105 °C is depicted in Fig. 18.

According to Fig. 18, it is observed that at 25 °C, the consumption rate of the fast-reacting mineral is not significant due to lower reactivity of the acid. At moderate temperature condition of 65 °C, the consumption rate of the fast-reacting mineral increases. When the temperature is very high at 105 °C, a drastic reduction in the composition of fast-reacting mineral is observed from the 3D numerical visualization results. This is because the acid reactivity is very high at such a high-temperature formation environment. Similar trend is obtained for the rate of silica gel precipitation or generation during the sandstone core flooding process as clearly shown in Fig. 18.

In this simulation, the fast-reacting mineral would be consumed throughout the acid–rock chemical reactions whereas the silica gel would be produced from the reaction between H_2SiF_6 and fast-reacting mineral. At the same time, silica gel would also be consumed in its reaction with HF. Tables 8 and 9 show the results of the effect of temperature on fast-reacting mineral and silica gel, respectively. The initial fast-reacting mineral volume fraction and silica gel volume fraction values are constant for various temperatures. These values are determined from the initial input to the simulation. Their respective response curves over acid injection time are also plotted graphically in Figs. 19 and 20.

According to Fig. 19, at 25 °C, the volume fraction of fast-reacting mineral slowly decreases upon consumption by both HF and H_2SiF_6. A less steep trend is observed from the graph along the acid injection time. However, as the formation temperature increases, the volume fraction response curve indicated that the reduction in fast-reacting mineral volume fraction becomes faster and more drastic. This is due to the higher rapidity of the chemical reactions. The higher the temperature, the faster the chemical equilibrium shifts to the right hand side. Hence, this causes more fast-reacting mineral dissolution.

Referring to Fig. 20, the precipitation of silica gel at 25 °C is not so much. Therefore, the increment of the silica gel volume fraction is not significant. Nevertheless at higher temperatures, the volume fraction of silica gel would also be getting higher. The trend of the volume fraction response curve became steeper, with an increased slope. Theoretically, this resulted from the higher acid–rock reactivity at higher temperature. Therefore, the equilibrium for the chemical reaction between H_2SiF_6 and fast-reacting mineral is shifting to the right hand side at a faster speed, forming more silica gel precipitate.

According to the overall increase in the silica gel precipitation, one could also understand that the chemical reaction between the H_2SiF_6 and fast-reacting mineral is more significant than the chemical reaction between HF and silica gel to produce H_2SiF_6, which would otherwise result in an overall decrease curve in the silica gel volume fraction. In
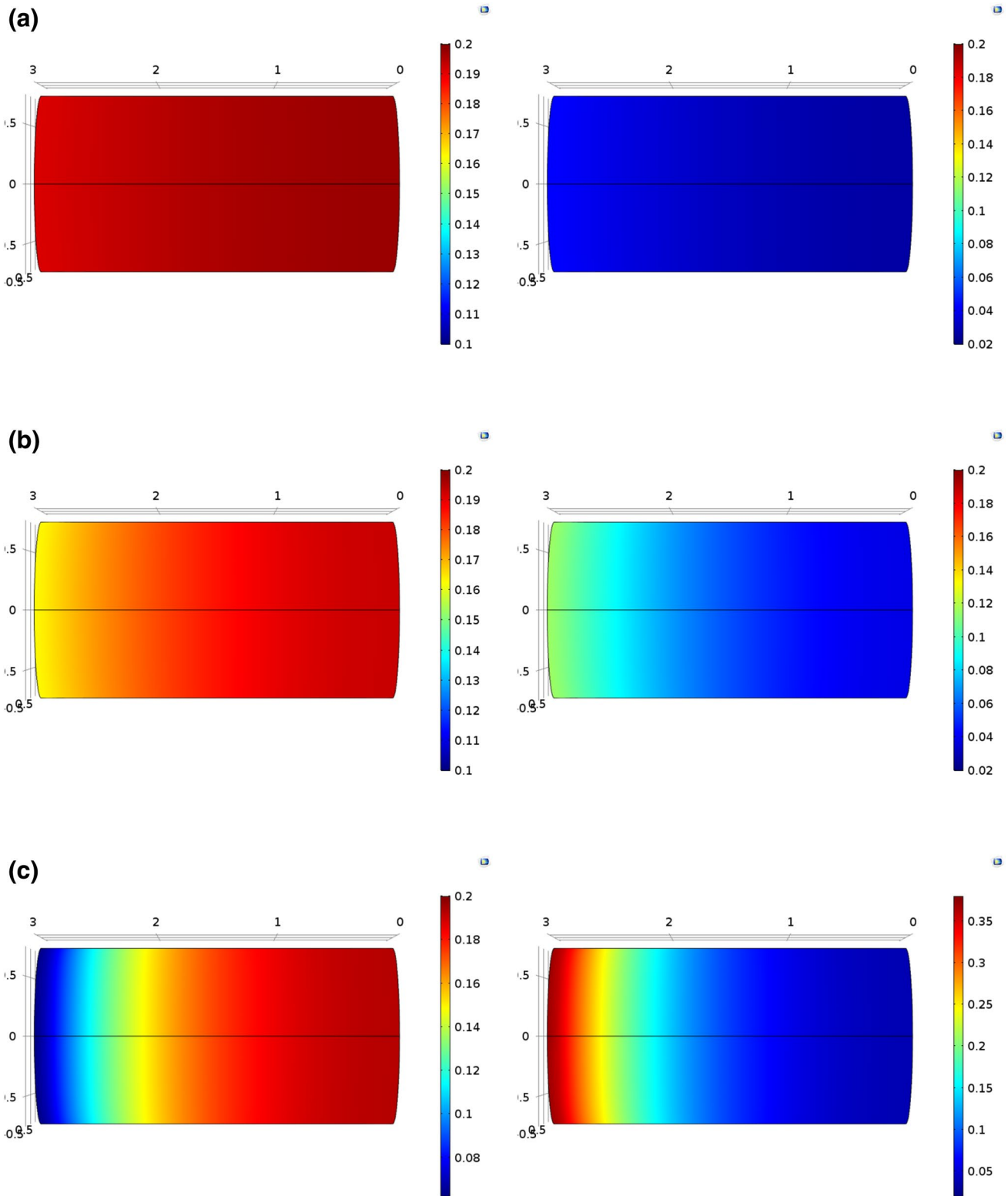
(a)

(b)

(c)

Fig. 18 Fast-reacting mineral (left) and silica gel (right) distribution after 35 min of fluoroboric acid injection at **a** 25 °C, **b** 65 °C and **c** 105 °C

Table 8 Effect of temperature on fast-reacting mineral volume fraction

Temperature, T (°C)	Initial fast-reacting mineral volume fraction	Final fast-reacting mineral volume fraction
25	0.2	0.1952
45	0.2	0.1907
65	0.2	0.1833
85	0.2	0.1727
105	0.2	0.1592

Table 9 Effect of temperature on silica gel volume fraction

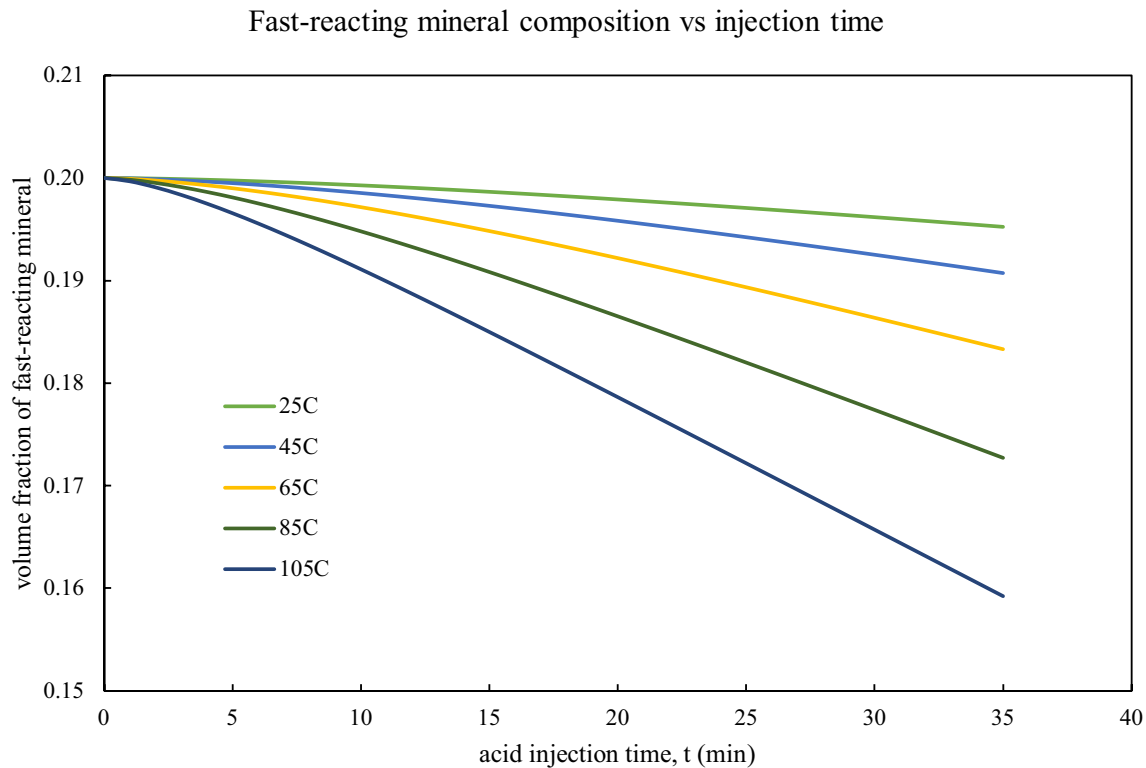| Temperature, T (°C)	Initial silica gel volume fraction	Final silica gel volume fraction
25	0.02	0.0323
45	0.02	0.0440
65	0.02	0.0631
85	0.02	0.0905
105	0.02	0.1253

other words, the rate of silica gel production is more rapid than the rate of silica gel consumption during the acid core flooding stimulation process.

Conclusion

A 3D mathematical model to simulate the performance of fluoroboric acid, HBF_4, at various range of temperatures had been developed. The numerical simulation process had also been accomplished using the COMSOL® Multiphysics commercial software of computational fluid dynamics (CFD). A finite element method (FEM) was adopted and implemented to perform the numerical solving of the core-scale cylindrical model. Finally, a number of 3D visualization of the simulation results as well as interpretation were presented. Based on the modelling results, there are a few conclusions that were drawn to attention as highlighted in the following points.

The model had been validated against the measured experimental data by Zhou et al. (2016) in the literature. The results of model verification at both 25 and 65 °C were highly satisfying. The plot data of permeability enhancement ratio over the acid injection time fit the experimental test data closely and consistently, indicating good agreement of the results. Therefore, the feasibility and reliability of the model in this study could be rest assured confidently.

The simulation results showed that porosity increases at low (25 °C), medium (65 °C) and high (105 °C) temperature conditions were 1.07, 1.26 and 1.67 times the initial value, respectively; whereas the permeability increases at

Fast-reacting mineral composition vs injection time

Fig. 19 The effect of temperatures on fast-reacting mineral composition over injection time

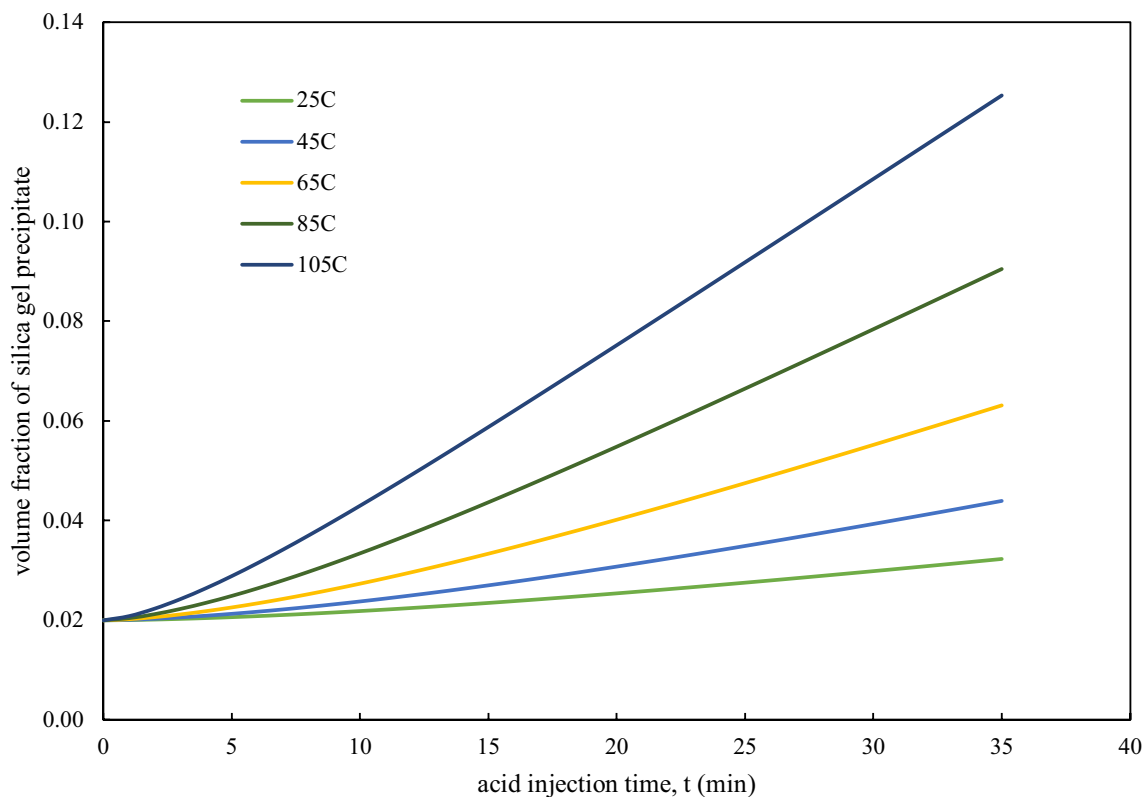## Silica gel precipitate composition vs injection time

Fig. 20 The effect of temperatures on silica gel precipitate composition over injection time

low (25 °C), medium (65 °C) and high (105 °C) temperature conditions were 1.23, 2.06 and 7.06 times the initial value, respectively. At room temperature, the porosity and permeability enhancement were not significant due to low hydrolysis rate that limits the acid penetration speed. When the temperature increases, the acid–rock chemical reaction shifts to the right more drastically, hence producing more HF to dissolve more mineral content. Then, this resulted in significant porosity and permeability improvement in the sandstone matrix.

Overall, it is concluded that the efficiency and performance of HBF_4 acid in sandstone matrix stimulation became better at increased temperature. In general, the hydrolysis reaction of HBF_4 that had been included in this model became the governing model that controlled the acid performance at various temperatures. In the future, it is recommended to optimize more other parameters, like acid concentration, mineral content and acid injection rate by adopting parametric study and sensitivity analysis using this model.

Appendix: Derivation of governing equations

Pressure equation

Figure 21 depicts a cubic control volume was defined in formulating the acidizing model.

Equation (21) shows the mass balance equation of the sandstone acid solution.

$$\text{Acid in} - \text{Acid out} + \text{Source} = \text{Accumulation} \qquad (21)$$
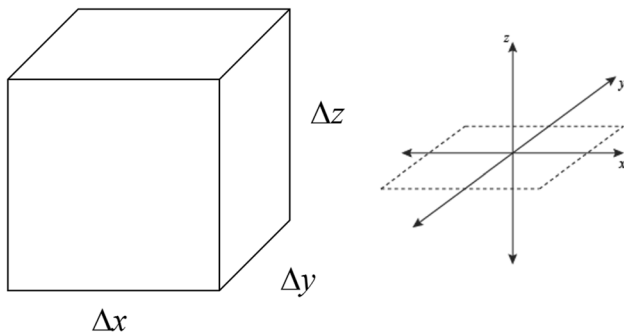
Fig. 21 The control volume of the acidizing model

The mass of acid solution flowing into the control volume is described in Eq. (22).

$$\Delta t\left(\left(\rho u_x \Delta y \Delta z\right)\Big|_x + \left(\rho u_y \Delta x \Delta z\right)\Big|_y + \left(\rho u_z \Delta y \Delta x\right)\Big|_z\right) \quad (22)$$

where ρ is the density of the acid solution; and u_x, u_y, and u_z are the average Darcy velocity in $y - z$ plane, $x - z$ plane and $x - y$ plane respectively.

The mass of acid solution flowing out from the control volume is described in Eq. (23).

$$\Delta t\left(\left(\rho u_x \Delta y \Delta z\right)\Big|_{x+\Delta x} + \left(\rho u_y \Delta x \Delta z\right)\Big|_{y+\Delta y} + \left(\rho u_z \Delta y \Delta x\right)\Big|_{z+\Delta z}\right) \quad (23)$$

Since the acid solution is assumed to be the only phase existing in the pore space of the sandstone core, the change in mass in the control volume over a period of time is defined in Eq. (24).

$$\Delta x \Delta y \Delta z\left((\rho\phi)^{t+\Delta t} - (\rho\phi)^t\right) \quad (24)$$

Assuming that during the acid injection, there is no source of acid solution in the core sample. Hence, the total acid solution flowing into the control volume equals to the accumulation of the acid solution. So, the expression of mass conservation of the acid solution is shown in Eq. (25).

The density of acid solution, ρ, is set as constant due to the assumption that stated the acid solution is incompressible. The limits of x, y, z and t were taken as $\Delta x \to 0$, $\Delta y \to 0$, $\Delta z \to 0$ and $\Delta t \to 0$. So, Eq. (26) can then be expressed as Eq. (27).

$$\frac{\partial \phi}{\partial t} = \frac{\partial u_x}{\partial x} + \frac{\partial u_y}{\partial y} + \frac{\partial u_z}{\partial z} \quad (27)$$

In vector form, it can be defined as Eq. (28).

$$\frac{\partial \phi}{\partial t} = \overline{\nabla} \cdot \bar{u} \quad (28)$$

where $\bar{u}$ is the velocity vector $\left\{u_x, u_y, u_z\right\}$, defined as the Darcy velocity in Eq. (29).

$$\bar{u} = -\frac{\bar{\bar{k}}}{\propto} \cdot \left(\overline{\nabla}P + \gamma \overline{\nabla}z\right) \quad (29)$$

where γ is the ratio of gravity. Since the gravitational effect is neglected, it can be expressed as Eq. (30).

$$\bar{u} = -\frac{\bar{\bar{k}}}{\propto} \cdot \overline{\nabla}P \quad (30)$$

Then, Eq. (31) is obtained by substituting Eq. (30) into Eq. (28).

$$\frac{\partial \phi}{\partial t} = \overline{\nabla} \cdot \left(-\frac{\bar{\bar{k}}}{\propto} \cdot \overline{\nabla}P\right) = -\frac{1}{\propto}\frac{\partial}{\partial x}\left(k_x \frac{\partial P}{\partial x}\right) - \frac{1}{\propto}\frac{\partial}{\partial y}\left(k_y \frac{\partial P}{\partial y}\right)$$
$$- \frac{1}{\propto}\frac{\partial}{\partial z}\left(k_z \frac{\partial P}{\partial z}\right) \quad (31)$$

When Eq. (31) is solved during the simulation, the porosity in each time step is kept constant. So, it is then simplified to Eq. (11).

$$\frac{1}{\propto}\frac{\partial}{\partial x}\left(k_x \frac{\partial P}{\partial x}\right) + \frac{1}{\propto}\frac{\partial}{\partial y}\left(k_y \frac{\partial P}{\partial y}\right) + \frac{1}{\propto}\frac{\partial}{\partial z}\left(k_z \frac{\partial P}{\partial z}\right) = 0 \quad (11)$$

$$\Delta x \Delta y \Delta z\left((\rho\phi)^{t+\Delta t} - (\rho\phi)^t\right) = \Delta t\left(\left(\rho u_x \Delta y \Delta z\right)\Big|_x + \left(\rho u_y \Delta x \Delta z\right)\Big|_y + \left(\rho u_z \Delta y \Delta x\right)\Big|_z\right)$$
$$- \Delta t\left(\left(\rho u_x \Delta y \Delta z\right)\Big|_{x+\Delta x} + \left(\rho u_y \Delta x \Delta z\right)\Big|_{y+\Delta y} + \left(\rho u_z \Delta y \Delta x\right)\Big|_{z+\Delta z}\right) \quad (25)$$

Equation (15) is then divided by $\Delta x \Delta y \Delta z \Delta t$ to become Eq. (26).

$$\frac{(\rho\phi)^{t+\Delta t} - (\rho\phi)^t}{\Delta t} = \frac{\left(\rho u_x\right)_x - \left(\rho u_x\right)_{x+\Delta x}}{\Delta x} + \frac{\left(\rho u_y\right)_y - \left(\rho u_y\right)_{y+\Delta y}}{\Delta y}$$
$$+ \frac{\left(\rho u_z\right)_z - \left(\rho u_z\right)_{z+\Delta z}}{\Delta z} \quad (26)$$

General material balance equation

Generally, the material balance equation for the model can be described as Eq. (32).

$$\frac{\partial W_i}{\partial t} + \overline{\nabla} \cdot \overline{N}_i = R_i \quad (32)$$

where

$$W_i = \phi \sum_{j=1}^{Np} \rho_j St_j \omega_{i,j} + (1-\phi)\rho_s \omega_{i,s} \qquad (33)$$

$$\overline{N}_i = \sum_{j=1}^{Np} u_j \rho_j \omega_{i,j} - \phi \sum St_j \rho_j \overline{\overline{k}}_{i,j} \cdot \overline{\nabla}\omega_{i,j} \qquad (34)$$

W_i is the overall mass of component i in the control volume, [=]g_i/bulk vol, $\omega_{i,j}$ mass fraction of component i in phase j, [=]$g_i/g_{\mathrm{phase}j}$, $\omega_{i,s}$ Mass fraction of component i in solid phase, [=]g_i/g_{solid}, ϕ Porosity, [=]pore vol/bulk vol, St_j saturation of phase j, [=]vol$_{\mathrm{phase}\,j}$/pore vol, ρ_j Density of phase j, [=]$g_{\mathrm{phase}j}$/vol$_{\mathrm{phase}j}$, ρ_s Density of solid, [=]g_{solid}/vol$_{\mathrm{solid}}$, N_i Flux of component i, [=]$g_i/L^2 - t$, u_j Darcy velocity of phase j, [=]L/t, $K_{i,j}$ dispersion coefficient of component i in phase j, [=] 1, R_i source of component i, [=]g_i/bulk vol $- t$, i Component index, j Phase index.

Mass conservation equation of acid components

Referring to Eq. (33), the mass component of i in the liquid phase is represented in the first term $\left(\phi \sum_{j=1}^{Np} \rho_j St_j \omega_{i,j}\right)$ on the right hand side whereas the mass component of i in the solid phase is represented in the second term $\left((1-\phi)\rho_s \omega_{i,s}\right)$ of the equation. Since the core flooding process is assumed as single-phase flow, then the term N_p and S_t become 1 and the subscript j can be neglected. Second, the second term on the right hand side of Eq. (33) can be cancelled out as no sorption on the solid phase is assumed during the acid treatment process. Finally, Eq. (33) had been simplified as Eq. (35).

$$W_i = \phi \rho \omega_i \qquad (35)$$

In the control volume of this simulation, the mass of acid i is considered in term of concentration, C_i. Therefore, the term $\rho \omega_i$ becomes C_i as shown in Eq. (36).

$$W_i = \phi C_i \qquad (36)$$

where C_i Concentration of acid i, [=] mol i/m^3 acid solution.

Referring to Eq. (34), the convection flow of component i is represented by the first term $\left(\sum_{j=1}^{Np} u_j \rho_j \omega_{i,j}\right)$ on the right hand side while the dispersion flow of component i is represented by the second term $\left(-\phi \sum St_j \rho_j \overline{\overline{k}}_{i,j} \cdot \overline{\nabla}\omega_{i,j}\right)$ on the equation. In the model, the effect of dispersion can be neglected from the equation as the spread of acid front is dominantly controlled by the chemical reactions between the acids and the minerals. Hence, assuming no dispersion, the second term on the right hand side of Eq. (34) can be cancelled thus simplifying the equation into Eq. (37).

$$\overline{N}_i = \bar{u}\rho\omega_i \qquad (37)$$

Similarly as Eq. (35), the mass balance term of acid i is being replaced with the concentration term, C_i as shown in Eq. (38).

$$\overline{N}_i = \bar{u}C_i \qquad (38)$$

Referring to Eq. (32), the source term on the right hand side, R_i is known as the reaction rate of acid i. So, Eq. (32) can be simplified by substituting Eqs. (36) and (38) into it and form a new expression for the mass conservation of the acid solution as shown in Eq. (39).

$$\frac{\partial(C_i\phi)}{\partial t} + \overline{\nabla} \cdot (\bar{u}C_i) = R_i \qquad (39)$$

where R_i the rate of appearance of acid i in the solution [=], $g_i/L^3 - t$.

So, the source term R_i in Eq. (39) is specifically the reaction rate of acid i whereas R_i in Eq. (32) represents the source in just a general way.

Generally, the definition of reaction rate is the speed at which a chemical reaction proceeds. In other words, it is the rate of appearance in the species solution at a specific period of time. This can be expressed in Eq. (40).

$$R_i = r_i S_j \qquad (40)$$

where r_i the surface area—specific reaction rate of i, [=]mol/s $- m^2$, S_j the surface area of mineral j in a unit of bulk volume, [=]$m^2/bulk\ vol$;

Usually, R_i is dependent on the concentration of the reacting species. So, it is expressed as Eq. (41).

$$-R_i = E_{f,i,j}C_i^\alpha S_j \qquad (41)$$

where $E_{f,i,j}$ are the reaction rate constant between acid i and mineral j, [=] mol $A/[m^2 - s - (mol\ A/m^3)]^\alpha$;

During the core flooding treatment, the acid is consumed and the rate of acid consumption in the solution is shown in Eq. (42).

$$R_i = -\sum_{j=1}^{N_m} E_{f,i,j}S_j^* V_j(1-\phi)C_i^\alpha \qquad (42)$$

where N_m the number of minerals reacting with acid i, S_j^* the specific surface area per unit volume of solid, [=]m^2/m^3, V_j the volume fraction for mineral j, [=] m^2 mineral j/m^3 solid volume.

Substituting Eq. (42) into (39) to yield Eq. (13).

$$\frac{\partial(C_i\phi)}{\partial t} + \overline{\nabla} \cdot (\bar{u}C_i) = -\sum_{j=1}^{N_m} E_{f,i,j}S_j^* V_j(1-\phi)C_i^\alpha \qquad i = 1, 2 \qquad (13)$$

Mass conservation equation of HF

HF is being used up by its reactions with three mineral groups. At the same time, it is continuously being produced as a result of HBF_4 hydrolysis. Hence the rate of HF generation equals to the rate of HBF_4 hydrolysis. So, the general material balance equation for HF ($i = 1$) is written as Eq. (43).

$$\frac{\partial(C_1\phi)}{\partial t} + \overline{\nabla} \cdot (\bar{u}C_1) = -\sum_{j=1}^{N_m} E_{f,1,j}S_j^*V_j(1-\phi)C_1^\alpha + r_h \quad (43)$$

Referring to Eq. (43), the terms at the left hand side represents the total change in mass of HF per unit time and sub-change in mass due to fluid transport whereas the terms at the right hand side is the sub-change in mass due to HF chemical reactions and HBF_4 hydrolysis.

During the sandstone acidizing, HF is commonly known to react with three mineral lumped group exist in a sandstone matrix. So, $N_m = 3$. In an expanded form, it can be written as Eq. (44).

$$\frac{\partial(C_1\phi)}{\partial t} + \overline{\nabla} \cdot (\bar{u}C_1) = -\big(E_{f,1,1}S_1^*V_1(1-\phi) \\ + E_{f,1,2}S_2^*V_2(1-\phi) + E_{f,1,3}S_3^*V_3(1-\phi)\big)C_1^\alpha + r_h \quad (44)$$

Assigning new terms C_{D1} and t_D into the equation. Let $C_{D1} = \frac{C_1}{C_1^0}$ and $t_D = \frac{ut}{\phi L}$, where C_1^0 is the initial concentration of HF, ϕ is the initial porosity and u is the velocity of injected acid. During the simulation, the acid concentration equation is solved such that the porosity, ϕ, is assumed to be constant throughout the process. The rate of injection, u is assumed to be constant too. Therefore, it is described as Eq. (45).

$$\frac{\phi C_1^0 \partial C_{D1}}{\frac{\phi L}{u}\partial t_D} + \overline{\nabla} \cdot (\bar{u}C_{D1}C_1^0) = r_h - \big(E_{f,1,1}S_1^*V_1(1-\phi) \\ + E_{f,1,2}S_2^*V_2(1-\phi) + E_{f,1,3}S_3^*V_3(1-\phi)\big)C_1^\alpha \quad (45)$$

Assuming α to be 1, it becomes Eq. (46).

$$\frac{\partial C_{D1}}{\partial t_D} + \overline{\nabla} \cdot \left(\frac{\bar{u}}{u}LC_{D1}\right) = r_h - \left(E_{f,1,1}S_1^*V_1 + E_{f,1,2}S_2^*V_2 + E_{f,1,3}S_3^*V_3^0\frac{V_3}{V_1^0}\right)C_{D1}\frac{L}{u}(1-\phi) \quad (46)$$

Let $\bar{u}_D = \frac{\bar{u}}{u}$ and $\overline{\nabla}_D = L \cdot \overline{\nabla} = \frac{\partial}{\partial x_D} + \frac{\partial}{\partial y_D} + \frac{\partial}{\partial z_D}$

$$\frac{\partial C_{D1}}{\partial t_D} + \overline{\nabla}_D \cdot \left(\bar{u}_D\overline{C}_{D1}\right) = r_h - \left(E_{f,1,1}S_1^*V_1^0\frac{V_1}{V_1^0} + E_{f,1,2}S_2^*V_2^0\frac{V_2}{V_2^0} + E_{f,1,3}S_3^*V_3^0\frac{V_3}{V_3^0}\right)C_{D1}\frac{L}{u}(1-\phi) \quad (47)$$

In the form of dimensionless equation, mass balance equation for HF is expressed as Eq. (48).

$$\frac{\partial C_{D1}}{\partial t_D} + \overline{\nabla}_D \cdot (\bar{u}_DC_{D1}) = r_h - \big(N_{Da,1}\Lambda_1 + N_{Da,2}\Lambda_2 + N_{Da,3}\Lambda_3\big)C_{D1} \quad (48)$$

The term N_{Da} is known as the Damkohler number. It is the ratio of the acid consumption rate to the acid convection rate. During the sandstone acid treatment, the specific surface area of the mineral is assumed constant. Hence, the Damkohler numbers of the reactions between HF and the three mineral groups are defined as Eqs. (49)–(51).

$$N_{Da,1} = \frac{E_{f,1,1}S_1^*V_1^0(1-\phi)L}{u} \quad (49)$$

$$N_{Da,2} = \frac{E_{f,1,2}S_2^*V_2^0(1-\phi)L}{u} \quad (50)$$

$$N_{Da,3} = \frac{E_{f,1,3}S_3^*V_3^0(1-\phi)L}{u} \quad (51)$$

The term Λ is called the dimensionless composition of mineral. The definition of the dimensionless volume fractions of the three groups of mineral are expressed in Eqs. (52)–(54).

$$\Lambda_1 = \frac{V_1}{V_1^0} \quad (52)$$

$$\Lambda_2 = \frac{V_2}{V_2^0} \quad (53)$$

$$\Lambda_3 = \frac{V_3}{V_3^0} \quad (54)$$

Mass conservation equation of H_2SiF_6

In the acid solution, the in situ product of the three chemical reactions between HF and the three reactive sandstone mineral groups, which is the fluorosilicic acid, H_2SiF_6 is also considered. Comparing to the HF, H_2SiF_6 also has a significant dissolving capacity. At the same time, H_2SiF_6 is the reactant of one reaction. It reacts with the fast-reacting

minerals to precipitate silica gel. Therefore, the mass balance equation of H_2SiF_6 ($i = 2$) is shown in Eq. (55).

$$\frac{\partial(C_2\phi)}{\partial t} + \overline{\nabla} \cdot (\bar{u}C_2) = -E_{f,2,1}S_1^*V_1(1-\phi)C_2^\alpha$$
$$+ \left(\frac{v_5}{v_1}E_{f,1,1}S_1^*V_1(1-\phi) + \frac{v_6}{v_2}E_{f,1,2}S_2^*V_2(1-\phi) + \frac{v_7}{v_3}E_{f,1,3}S_3^*V_3(1-\phi)\right)C_1^\alpha \tag{55}$$

The term v_i is the stoichiometric coefficient described in the chemical reaction model in "Chemical reaction model" section. Their values are determined from the previously done experimental investigations.

Assigning new terms C_{D2} and t_D into the equation. Let $C_{D2} = \frac{C_2}{C_1^0}$ and $t_D = \frac{ut}{\phi L}$, Eq. (56) is being defined as follows:

$$\frac{\phi C_1^0 \partial C_{D2}}{\frac{\phi L}{u}\partial t_D} + \overline{\nabla} \cdot (\bar{u}C_{D2}C_1^0) = -\left(E_{f,2,1}S_1^*V_1(1-\phi)\right)C_2^\alpha$$
$$+ \left(\frac{v_5}{v_1}E_{f,1,1}S_1^*V_1(1-\phi) + \frac{v_6}{v_2}E_{f,1,2}S_2^*V_2(1-\phi) + \frac{v_7}{v_3}E_{f,1,3}S_3^*V_3(1-\phi)\right)C_1^\alpha \tag{56}$$

Assuming α to be 1, it becomes Eq. (57).

$$\frac{\partial C_{D2}}{\partial t_D} + \overline{\nabla}_D \cdot \left(\frac{\bar{u}}{u}C_{D2}\right) = -\left(E_{f,2,1}S_1^*V_1^0(1-\phi)\right)C_{D2}\frac{V_1}{V_1^0}\frac{L}{u}$$
$$+ \begin{pmatrix} \frac{v_5}{v_1}E_{f,1,1}S_1^*V_1^0(1-\phi)\frac{V_1}{V_1^0} + \frac{v_6}{v_2}E_{f,1,2}S_2^*V_2^0(1-\phi)\frac{V_2}{V_2^0} \\ +\frac{v_7}{v_3}E_{f,1,3}S_3^*V_3^0(1-\phi)\frac{V_3}{V_3^0} \end{pmatrix} C_{D1}\frac{L}{u} \tag{57}$$

In the form of dimensionless equation, mass balance equation for H_2SiF_6 is expressed as Eq. (58).

$$\frac{\partial C_{D2}}{\partial t_D} + \overline{\nabla}_D \cdot (\bar{u}_D C_{D2}) = -N_{Da,4}\Lambda_1 C_{D1} + \left(\frac{v_5}{v_1}N_{Da,1}\Lambda_1 + \frac{v_6}{v_2}N_{Da,2}\Lambda_2 + \frac{v_7}{v_3}N_{Da,3}\Lambda_3\right)C_{D1} \tag{58}$$

The Damkohler number for the reaction between H_2SiF_6 and the fast-reacting minerals, $N_{Da,4}$, is defined in Eq. (59).

$$N_{Da,4} = \frac{E_{f,2,1}S_1^*V_1^0(1-\phi)L}{u} \tag{59}$$

Mass conservation equation of minerals

The term $\left(\left(\phi \sum_{j=1}^{Np} \rho_j St_j \omega_{i,j}\right)\right)$ in Eq. (33) can be cancelled out and $(1-\phi)V_j$ corresponds to the amount of mineral j that appear in solid phase. Also, assuming that there is no flow of solid phase, the term $\overline{\nabla} \cdot \overline{N}_i$ is removed from Eq. (32). The source term R_i in Eq. (32) represents the rate of reaction of

mineral j during the core flooding. It is determined by the rate of reaction and dissolving power of the acid. The dissolving power of acid is defined as the amount of mineral that is reacted and consumed by a specific amount of acid. In the basis of mass, it can be written as Eq. (60).

$$\beta = \frac{v_{mineral}MW_{mineral}}{v_{acid}MW_{acid}} \tag{60}$$

Mass conservation equation of fast-reacting minerals

Based on the general material balance equation for minerals, the dimensionless form of material balance for all the three minerals has been developed. First, the fast-reacting mineral ($j = 1$) is being dissolved by both the acids, HF and H_2SiF_6. So, the mass balance of fast-reacting mineral is expressed as Eq. (61).

$$\frac{\partial\left((1-\phi)V_1\right)}{\partial t} = -\frac{MW_{HF}S_1^*V_1(1-\phi)\beta_{HF,1}E_{f,HF,1}C_{HF}}{\rho_1}$$
$$-\frac{MW_{H_2SiF_6}S_1^*V_1(1-\phi)\beta_{H_2SiF_6,1}E_{f,H_2SiF_6,1}C_{H_2SiF_6}}{\rho_1} \tag{61}$$

Similarly, the porosity is considered as constant in the reaction process as shown in Eq. (62).

$$\frac{\partial V_1}{\partial t} = -\left(MW_{HF}\beta_{HF,1}E_{f,HF,1}C_{HF} + MW_{H_2SiF_6}\beta_{H_2SiF_6,1}E_{f,H_2SiF_6,1}C_{H_2SiF_6}\right)\frac{S_1^*V_1}{\rho_1} \tag{62}$$

Then, the dimensionless volume fraction of fast-reacting mineral defined in Eq. (52) and dimensionless time are substituted into the equation and written as Eq. (63).

$$\frac{\partial\Lambda_1}{\partial t_D} = -\left(MW_{HF}\beta_{HF,1}E_{f,HF,1}C_{HF} + MW_{H_2SiF_6}\beta_{H_2SiF_6,1}E_{f,H_2SiF_6,1}C_{H_2SiF_6}\right)\frac{S_1^*V_1\phi L}{\rho_1 u V_1^0}$$

$$= -\left(\begin{array}{l} \dfrac{(1-\phi)V_1^0E_{f,HF,1}S_1^*L}{u} \cdot \dfrac{1}{(1-\phi)V_1^0} \cdot \dfrac{\phi MW_{HF}C_{HF}^0\beta_{HF,1}}{\rho_1}\dfrac{C_{HF}}{C_{HF}^0} \\ + \dfrac{(1-\phi)V_1^0E_{f,H_2SiF_6,1}S_1^*L}{u} \cdot \dfrac{1}{(1-\phi)V_1^0} \cdot \dfrac{\phi MW_{HF}C_{HF}^0\beta_{H_2SiF_6,1}}{\rho_1}\dfrac{C_{H_2SiF_6}}{C_{HF}^0} \end{array} \right)\dfrac{V_1}{V_1^0} \tag{63}$$

Considering the Damkohler numbers as shown in Eqs. (49) and (59), the equation is further simplified into Eq. (64).

$$\frac{\partial\Lambda_1}{\partial t_D} = -\left(N_{Da,1} \cdot N_{Ac,1} \cdot C_{D1} + N_{Da,4} \cdot N_{Ac,4} \cdot C_{D2}\right) \cdot \Lambda_1 \tag{64}$$

The term N_{Ac} is a dimensionless number known as the acid capacity number. The definition of N_{Ac} is the ratio of the amount of mineral consumed by the acid in a volumetric pore space to the amount of mineral exist in the volumetric sandstone matrix. The acid capacity number for the reaction

$$N_{Ac,1} = \frac{\phi C_{HF}^0 MW_{HF}\beta_{HF,1}}{(1-\phi)V_1^0\rho_1} \tag{65}$$

$$N_{Ac,4} = \frac{\phi C_{HF}^0 MW_{H_2SiF_6}\beta_{H_2SiF_6,1}}{(1-\phi)V_1^0\rho_1} \tag{66}$$

Mass conservation equation of slow-reacting minerals

As shown in the chemical reaction model, the slow-reacting mineral ($j=2$) only reacts with HF. Thus, the material balance is written in the form of Eq. (67).

$$\frac{\partial\left((1-\phi)V_2\right)}{\partial t} = -\frac{MW_{HF}S_2^*V_2(1-\phi)\beta_{HF,2}E_{f,HF,2}C_{HF}}{\rho_2} \tag{67}$$

Taking the porosity as a constant in the reaction, it becomes Eq. (68).

$$\frac{\partial V_2}{\partial t} = -\left(MW_{HF}\beta_{HF,2}E_{f,HF,2}C_{HF}\right)\frac{S_2^*V_2}{\rho_2} \tag{68}$$

After that, the dimensionless volume fraction of slow-reacting mineral defined in Eq. (53) and dimensionless time are substituted into the equation, forming Eq. (69).

$$\frac{\partial\Lambda_2}{\partial t_D} = -\left(\frac{MW_{HF}S_2^*V_2\beta_{HF,2}E_{f,HF,2}C_{HF}}{\rho_2}\right)\frac{\phi L}{u V_2^0}$$
$$= -\left(\frac{(1-\phi)V_2^0E_{f,HF,2}S_2^*L}{u} \cdot \frac{1}{(1-\phi)V_2^0} \cdot \frac{\phi MW_{HF}C_{HF}^0\beta_{HF,2}}{\rho_2}\frac{C_{HF}}{C_{HF}^0}\right)\frac{V_2}{V_2^0} \tag{69}$$

Substituting the Damkohler numbers from Eq. (50) into it, the simplified Eq. (70) is formed.

$$\frac{\partial\Lambda_2}{\partial t_D} = N_{Da,2}N_{Ac,2}\Lambda_2 C_{D1} \tag{70}$$

Then, the acid capacity number for the reaction between HF and the slow-reacting mineral is formulated as Eq. (71).

between HF and fast-reacting mineral; and between H_2SiF_6 and fast-reacting mineral is expressed in Eqs. (65) and (66) respectively.

$$N_{Ac,2} = \frac{\phi C_{HF}^0 MW_{HF} \beta_{HF,2}}{(1-\phi)V_2^0 \rho_2} \tag{71}$$

Mass conservation equation of silica gel

The precipitated product, which is the silica gel is considered as mineral 3 in this model ($j = 3$). It is being reacted with HF during the acid injection but at the same time, it is being produced when H_2SiF_6 reacts with the fast-reacting minerals. The amount of silica gel being generated can be determined from the amount of fast-reacting minerals removed as well as the stoichiometry of the reaction.

$$\frac{\partial\big((1-\phi)V_3\big)}{\partial t} = -\frac{MW_{HF}S_3^*V_3(1-\phi)\beta_{HF,3}E_{f,HF,3}C_{HF}}{\rho_3} + \frac{MW_{H_2SiF_6}S_1^*V_1(1-\phi)\beta_{H_2SiF_6,1}E_{f,H_2SiF_6,1}C_{H_2SiF_6}}{\rho_3}\frac{v_8MW_3}{MW_1} \tag{72}$$

Based on Eq. (72), the term $S_1^*V_1(1-\phi)E_{f,H_2SiF_6,1}C_{H_2SiF_6}$ is the number of moles of H_2SiF_6 being reacted or consumed. The term $MW_{H_2SiF_6}S_1^*V_1(1-\phi)\beta_{H_2SiF_6,1}E_{f,H_2SiF_6,1}C_{H_2SiF_6}$ corresponds to the mass of removed or dissolved fast-reacting mineral by H_2SiF_6 per unit volume whereas the term $\frac{MW_{H_2SiF_6}S_1^*V_1(1-\phi)\beta_{H_2SiF_6,1}E_{f,H_2SiF_6,1}C_{H_2SiF_6}}{\rho_3}\frac{v_8MW_3}{MW_1}$ represents the volume of silica gel that is being precipitated during the reaction between H_2SiF_6 and the fast-reacting mineral.

Considering the porosity being constant in the reaction, Eq. (73) is developed.

$$\frac{\partial V_3}{\partial t} = -\big(MW_{HF}\beta_{HF,3}E_{f,HF,3}C_{HF}\big)\frac{S_3^*V_3}{\rho_3} + \big(MW_{H_2SiF_6}\beta_{H_2SiF_6,1}E_{f,H_2SiF_6,1}C_{H_2SiF_6}\big)\frac{v_8MW_3}{MW_1}\frac{S_1^*V_1}{\rho_3} \tag{73}$$

Substituting the dimensionless volume fraction of silica gel defined in Eqs. (52) and (54); and dimensionless time into the equation, Eq. (74) is formed.

Substituting the Damkohler numbers from Eqs. (51) and (59) into it, the equation is simplified to become Eq. (75).

$$\frac{\partial\Lambda_3}{\partial t_D} = -N_{Da,3}\cdot N_{Ac,3}\cdot\Lambda_3\cdot C_{D1} + N_{Da,4}\cdot N_{Ac,4}\cdot\Lambda_1\cdot C_{D2}\frac{v_8MW_3}{MW_1}\frac{\rho_1}{\rho_3} \tag{75}$$

The acid capacity number for the reaction between HF and the silica gel is expressed in Eq. (76).

$$N_{Ac,3} = \frac{\phi C_{HF}^0 MW_{HF}\beta_{HF,3}}{(1-\phi)V_1^0\rho_3} \tag{76}$$

Change in porosity

In expanded form, the porosity equation can be written as Eq. (77).

$$\frac{\partial\phi}{\partial t} = -\frac{MW_{HF}S_1^*V_1\beta_{HF,1}E_{f,HF,1}C_{HF}}{\rho_1} - \frac{MW_{H_2SiF_6}S_1^*V_1\beta_{H_2SiF_6,1}E_{f,H_2SiF_6,1}C_{H_2SiF_6}}{\rho_1} - \frac{MW_{HF}S_2^*V_2\beta_{HF,2}E_{f,HF,2}C_{HF}}{\rho_2} - \frac{MW_{HF}S_3^*V_3\beta_{HF,3}E_{f,HF,3}C_{HF}}{\rho_3} + \frac{MW_{H_2SiF_6}S_1^*V_1\beta_{H_2SiF_6,1}E_{f,H_2SiF_6,1}C_{H_2SiF_6}}{\rho_3}\frac{v_8MW_3}{MW_1} \tag{77}$$

$$\frac{\partial\Lambda_3}{\partial t_D} = -\left(\begin{array}{l}MW_{HF}\beta_{HF,3}E_{f,HF,3}C_{HF}\dfrac{S_3^*V_3}{\rho_3}\\[2mm] -MW_{H_2SiF_6}\beta_{H_2SiF_6,1}E_{f,H_2SiF_6,1}C_{H_2SiF_6}S_1^*V_1\dfrac{v_8MW_3}{MW_1\rho_3}\end{array}\right)\frac{\phi L}{uV_1^0}$$
$$= -\frac{(1-\phi)V_1^0 E_{f,HF,3}S_3^*L}{u}\cdot\frac{1}{(1-\phi)V_1^0}\cdot\frac{\phi MW_{HF}C_{HF}^0\beta_{HF,3}}{\rho_3}\frac{C_{HF}}{C_{HF}^0}\cdot\frac{V_3}{V_1^0}$$
$$+ \frac{(1-\phi)V_1^0 E_{f,H_2SiF_6,1}S_1^*L}{u}\cdot\frac{1}{(1-\phi)V_1^0}\cdot\frac{\phi MW_{H_2SiF_6}C_{HF}^0\beta_{H_2SiF_6,1}}{\rho_1}\frac{C_{H_2SiF_6}}{C_{HF}^0}\cdot\frac{V_1}{V_1^0}\frac{v_8MW_3}{MW_1}\frac{\rho_1}{\rho_3} \tag{74}$$

Initial conditions

In dimensionless form, the initial conditions solving the equations are written as Eq. (78).

$$\left.\begin{array}{c} C_{D,1} = C_{D,2} = 0 \\ \Lambda_1 = \Lambda_2 = \Lambda_3 = 1 \\ \phi = \phi^0 \end{array}\right\} \qquad \text{at } t_D = 0 \qquad (78)$$

Boundary conditions

In dimensionless form, the boundary conditions applied in the simulation are expressed as Eqs. (79)–(81).

$$\left.\begin{array}{c} C_{D,1} = 1 \\ Q = \text{Constant} \end{array}\right\} \qquad \text{at } x_D = 0 \qquad (79)$$

$$P = P_{\text{out}} \qquad \text{at } x_D = 1 \qquad (80)$$

$$\frac{\partial P}{\partial r} = 0 \qquad \text{at } r = r_c \qquad (81)$$

References

Al-Shaalan TM, Nasr-El-Din HA (2000) Mathematical modeling of sandstone stimulation: a critical review of available models. In: Proceedings of CORROSION 2000, NACE International, Orlando, Florida, 26–31 March 2000

Bertaux J (1989) Treatment-fluid selection for sandstone acidizing: permeability impairment in potassic mineral sandstones. SPE Prod Eng 4(1):41–48

Bryant SL (1993) An improved model of mud acid/sandstone chemistry. In: Proceedings of SPE annual technical conference and exhibition, Society of Petroleum Engineers, Dallas, Texas, 6–9 October 1993

Da Motta EP, Plavnik B, Schecter RS, Hill AD (1993) Accounting for silica precipitation in the design of sandstone acidizing. Soc Petrol Eng 8:138–144

Economides MJ, Hill AD, Ehlig-Economides C, Zhu D (2013) Petroleum production systems, 2nd edn. Prentice Hall, Upper Saddle River

Hekim Y, Fogler HS, McCune CC (1982) The radial movement of permeability fronts and multiple reaction zones in porous media. Soc Petrol Eng 22:99–107

Kume N, Luckie RVM E (1999) New HF acid system improves sandstone matrix acidizing success ratio by 400% over conventional mud acid system in niger delta basin. In: Proceedings, SPE annual technical conference and exhibition, Houston, Texas

Labrid JC (1975) Thermodynamic and kinetic aspects of argillaceous sandstone acidizing. Soc Petrol Eng 15:117–128

Leong VH, Ben Mahmud H (2017) A comparative study of different acids used for sandstone acid stimulation: a literature review. IOP Conf Ser Mater Sci Eng 217:012018. https://doi.org/10.1088/1757-899X/217/1/012018

Leong VH, Ben Mahmud H (2018) A preliminary screening and characterization of suitable acids for sandstone matrix acidizing technique: a comprehensive review. J Petrol Explor Prod Technol. https://doi.org/10.1007/s13202-018-0496-6

Leong VH, Mahmud B, Law H, Foo MC, H. C. Y. & Tan IS (2018) A comparison and assessment of the modelling and simulation of the sandstone matrix acidizing process: a critical methodology study. J Nat Gas Sci Eng 57:52–67. https://doi.org/10.1016/j.jngse.2018.06.044

Li C, Xie T, Pournik M, Zhu D, Hill AD (2004) Fine-scale simulation of sandstone acidizing. Soc Petrol Eng 127:225–232

Lin W, Chen L, Lu Y, Hu H, Liu l, Liu X, Wei W (2017) Diagenesis and its impact on reservoir quality for the Chang 8 oil group tight sandstone of the Yanchang formation (upper Triassic) in southwestern Ordos basin, China. J Petrol Explor Prod Technol 7:947. https://doi.org/10.1007/s13202-017-0340-4

Lindsay DM (1976) An experimental study of sandstone acidization, Report No. UT 76–1. Texas Petroleum Research Committee, Austin

Lund K, Fogler HS, Ault JW (1975) A new model of the physical and chemical changes in sandstone during acidizing. SPEJ 15:361–370

McLeod HO (1984) Matrix acidizing. Soc Petrol Eng 36:2055–2069

Paccaloni G, Mauro T (1993) Advances in matrix stimulation technology. J Petrol Technol 45(3):256–263

Restrepo A, Manuel L, Arthur WM (2012) Effective kaolinite damage control under unfavorable chemical environment: field case. In: Proceedings of SPE international symposium and exhibition on formation damage control, Lafayette, Louisiana

Ryss IG (1956) The chemistry of fluorine and its inorganic compounds. Moscow, State Publishing House of Scientific, Technical. In: and Literature C (Reprint).Eng. trans., AEC-tr-3927. Office of Technical Services, U.S. Dept. of Commerce, Washington D.C., 1960

Schechter RS, Gidley JL (1969) The change in pore size distribution from surface reactions in porous media. AIChEJ 15(2):339–350

Sevougian SD, Lake LW, Schechter RS (1995) A new geochemical simulator to design more effective sandstone acidizing treatments. Soc Petrol Eng 10:13–19

Shafiq MU, Mahmud B, H. K (2017) Sandstone matrix acidizing knowledge and future development. J Petrol Explor Prod Technol 7:1205. https://doi.org/10.1007/s13202-017-0314-6

Smith CF, Hendrickson AR (1965) Hydrofluoric acid stimulation of sandstone reservoirs. Soc Petrol Eng 17:215–222

Thomas RL, Crowe CW (1978) Single-stage chemical treatment provides stimulation and clay control in sandstone formations. In: Proceedings of SPE California regional meeting, Society of Petroleum Engineers, San Francisco, California, 12–14 April 1978

Thomas RL, Crowe CW (1981) Matrix treatment employs new acid system for stimulation and control of fines migration in sandstone formations. Soc Petrol Eng 33: 1–491

Walsh JB, Brace WF (1984) The effect of pressure on porosity and the transport properties of rock. J Geophys Res 89:9425–9431

Wamser CA (1948) Hydrolysis of fluoboric acid in aqueous solution. J Am Chem Soc 70(3):1209–1215 (83)

Wamser CA (1951) Equilibria in the system boron trifluoride—water at 25°. J Am Chem Soc 73(1):409–416

Zhou X, Zhang SC, Zhang X, Wang F, Lin H (2016) Core-scale experimental and numerical investigation on fluoroboric acidizing of a sandstone reservoir. Energy Technol 4: 870–879